

POLITECNICO DI TORINO  
Repository ISTITUZIONALE

Silica Aerogel: ISRU, Architecture and Applications for Mars and Space Settlements

*Original*

Silica Aerogel: ISRU, Architecture and Applications for Mars and Space Settlements / Lutz, Kolemman; Pino, Paolo; Bheekhun, Nadiir. - ELETTRONICO. - (2021). (Intervento presentato al convegno 72nd International Astronautical Congress tenutosi a Dubai, United Arab Emirates).

*Availability:*

This version is available at: 11583/2973786 since: 2022-12-13T10:13:28Z

*Publisher:*

IAF

*Published*

DOI:

*Terms of use:*

This article is made available under terms and conditions as specified in the corresponding bibliographic description in the repository

*Publisher copyright*

IAF/IAF postprint versione editoriale/Version of Record

Manuscript presented at the 72nd International Astronautical Congress, Dubai, United Arab Emirates, 2021. Copyright by IAF

(Article begins on next page)

## Silica Aerogel: ISRU, Engineering, and Applications for Mars and Space Settlements

Kolemann Lutz<sup>a</sup>, Paolo Pino<sup>b</sup>, Nadiir Bheekhun, PhD<sup>c</sup>

<sup>a</sup> *Cofounder, Mars University, Washington, DC, United States, kole@mars.university*

<sup>b</sup> *PhD Researcher, Politecnico di Torino, Turin, Italy, paolo.pino@polito.it*

<sup>c</sup> *Founder and Director, Aeronad, Port Louis, Mauritius, nadiir@aeronad.com*

### Abstract

This research evaluates the methods, materials science properties, applications of the silica (SiO<sub>2</sub>) and aerogel life cycle on Earth in the early to mid stages of a Mars and space settlement. Silica Aerogels (SA) are highly effective insulation and thermal materials for rovers, EDL vehicles, heat shields, cryotanks, habitats, spacesuits, domes, radiators, electronics, and regolith/soil heating. SA is also an effective material to improve the performance of inflatables, pipes, heavy metal absorbents, sensors, nuclear waste containment, filtration, and bioengineering. Methods to tailor the physical, mechanical, chemical, hydrophobic properties and radiation refractive index of SA are reviewed. The addition of carbon fiber nanoparticles can increase the compressive modulus of SA by three fold and tensile stress by five fold. Nanofabrication and synthesis methods are referenced including the crosslinking with polymers, and deposition with sprayable coatings.

Available data on hydrated silica bound minerals, maps, and native Martian minerals are referenced in candidate locations including Arcadia Planitia and Valles Marineris, paving a roadmap for industrial scale SiO<sub>2</sub>-based in-situ resource utilisation (ISRU) operations. Both the artificial and biological processes for the mining, extraction, separation, purification of silica and precursors from regolith are cited. The biogenic silica production on Earth with photosynthetic algae diatoms, radiolarians, sponges, and silicate solubilizing bacteria (SSB) are reviewed as novel organisms to biomine and produce SiO<sub>2</sub>. Microbial cell factories and algal photobioreactors also hold great potential to manufacture biomass, biodiesel, protein and bioplastics in situ.

A 2-3 cm thick layer of silica (SiO<sub>2</sub>) aerogel could shield almost all of the high-cancerous-levels of UVA, UVB, and UVC radiation in the space environment without an external heat source. As a key motivator for the research study, SiO<sub>2</sub> aerogel sheets hold the potential to enable water ice mining and provide habitable environments for cyanobacteria, algae, and biomass cultivation while simultaneously transmitting visible light for photosynthesis, blocking ultraviolet radiation, raising temperatures, and reducing energy costs to induce solid state greenhouse effects. This research provides a literature review with over 130 references to design the silica ISRU and aerogel production process. This study investigates the past, present, and future engineering applications, challenges, and advancements of SiO<sub>2</sub> aerogel to enable industrial scale production and habitable environments throughout the Solar system and beyond.

**Keywords:** Silica Aerogel, Greenhouse, Algae Mats, Space Settlement, In Situ Resource Utilisation

### Nomenclature

ASR = Alkali-Silica Reactivity

CRR = Carbothermal Reduction reactor

CVD = Chemical Vapor Deposition

HIRMS = High Intensity Rolling Magnetic separator

GCR = Galactic Cosmic Rays

ISRU = In Situ Resource Utilisation

IRMS = Induced Roller Magnetic Separation

PEG = Polyethylene Glycol

PI = Cross linked Polyimide

SA = Silica Aerogel

SSB = Silicate solubilizing Bacteria

TMOS = Tetramethyl Orthosilicate

## 1. Introduction

### 1.1. Challenges for Space Exploration and Settlement

Extreme thermal, radiative and atmospheric conditions pose challenges to the expansion of humans and life in space, celestial bodies, and throughout the Universe as most biology as we know it has not evolved to survive far from Earth. Aerogels and other insulative materials are highly effective at maintaining thermal operating environments for biological and nonbiological systems and mitigating heat loss to keep on-board electronics at approximately 20° C. With high cryogenic temperature gradients in space, Moon, Mars, and other celestial bodies, the typical temperature range for space-qualified electronics components is -55° C to +125° C with a 15° C margin on each side (-40° C to +110° C). As heaters are typically required to keep rovers and machine's battery systems from freezing, these external or self-heating components in energy storage devices add weight and constantly require power for instruments and machinery. Lithium ion batteries and supercapacitors typically have the lowest operating temperatures of -20° C to -40° C, limited by freezing points of electrolytes. These challenges suggest a need to identify, implement, and advance alternative methods and insulative thermal materials to expand operating temperature.

### 1.2. Silica Aerogel Material Properties

Silica (SiO<sub>2</sub>) is chemically stable and refractory (resistant to decomposition) at extreme temperatures and high thermal gradients such as those on the Moon, Mars, and vacuum of space. Silica aerogels (SA) are nanoporous networks of silicon dioxide (SiO<sub>2</sub>). The physical properties of SA's are highlighted in detail in Table 1 from a 2008 study on Silica Aerogel; Synthesis, Properties and Characterization [1]. Considering the high density of silica around 2200 kg/m<sup>3</sup> or 0.003-0.35 g/cm<sup>3</sup>, the aerogel's peculiar porous structure forms one of the lightest materials, around 50–200 kg/m<sup>3</sup> in mass with 5% solid fraction. The SA pore size ranges from 5–100 nm and constitute up to 99.9% of the total volume, which provides aerogel with spectacular thermal insulative properties with an extremely low thermal conductivity from 0.03 W·m<sup>-1</sup>·K<sup>-1</sup> [2] in atmospheric pressure to as low as 0.004 W·m<sup>-1</sup>·K<sup>-1</sup> in a modest vacuum. SiO<sub>2</sub> aerogel has a high R-values of R14 to R105 (US customary) or 3.0 to 22.2 (metric) for 3.5 in (89 mm) thickness, making it highly resistant to the conductive flow of heat. Aerogels used in applications for buildings on Earth have densities closer to 150kg/m<sup>3</sup> [3] and require specific surface areas of up to 500 m<sup>2</sup>/g·m [4].

Properties	Values	Properties	Values
Density (kg/m <sup>3</sup> )	3-350 (most common~100)	Primary particle diameter (nm)	2-5
Pore diameter (nm)	1-100 (~20 on average)	Surface area (m <sup>2</sup> /g)	600-1000
Porosity (%)	85-99.9 (typical ~ 95)	Index of refraction	1.0-1.05
Thermal conductivity (W/m K)	0.01-0.02	Thermal tolerance temperature (°C)	500 (m.p >1200)
Transmittance in 0.5-2.5µm, 3.7-5.9 µm	0.80-0.95	Coefficient of linear expansion (1/°C)	2.0-4.0 × 10 <sup>-6</sup>
Longitudinal sound speed (m/s)	100-300	Tensile strength (kPa)	16

Table 1. Physical properties of silica aerogel. [4]

The poor mechanical properties of silica aerogel result in a material that is typically extremely stiff and brittle [5,6], even though SiO<sub>2</sub> aerogel can sustain loads up to 2000X its weight in applied force. When forces are not applied gently and uniformly, the aerogel tends to fragment and pulverize. Moreover, the vibrations induced from a launch vehicle and entry descent and landing (EDL) could impose fractures and cracks in aerogel if not monitored, which could result in system and mission failure in extreme environments. Therefore, other materials, polymers such as plastic can be used to improve performance with lower elastic young's modulus (E) and rupture modulus (σ), or the measure of stress before it yields in a bend test.

### 1.3 Aerogels, Insulation, and Coatings to Attenuate Radiation

On Earth, humans are exposed to 3 to 4 millisieverts (mSv) of ionising radiation a year, mostly from natural sources like some kinds of rocks and the minimal galactic cosmic rays (GCR) through the atmosphere. Based on measurements made by the Curiosity rover, the average natural radiation level on Mars for the surface of Mars is approximately 230 mSv/year. [7] which is about 60-70X greater than the average on Earth. On the Moon, the annual exposure caused by GCR on the lunar surface is roughly 380 mSv (solar minimum) and 110 mSv (solar maximum) [8]. Astronauts on the lunar surface in an uninsulated environment without radiation protection would absorb 1,369 microsieverts per day, which is about 200 times the amount organisms receive on Earth's surface.

Solid silica is transparent to visible radiation but opaque to UV wavelengths shorter than 200-400 nm, and to infrared wavelengths longer than 2  $\mu\text{m}$ . Thus, aerogels hold great potential to block ionising UV-B, which damages DNA from sunlight wavelengths less than 320 nm and UV-C Radiation [9]. In a 1996 study, silica aerogel Cherenkov nuclear radiators samples were irradiated up to 9.8 Mrad of equivalent dose. Deteriorations in transparency and changes of refractive index were observed to be less than 1.3% and 0.001 at 90% confidence level, respectively. Thus, Silica aerogels can be used in high-radiation environments, such as B-factories, nuclear and heavy-ion experiments, space-station and satellite experiments, without any fear of radiation damage (Sahu, 1996). However, aerogel alone is generally not suitable to attenuate GCR's, protons, and gamma rays that bombard the Martian surface with intensities around 156.4 mSv/year (at solar maximum) to 273.8 mSv/year (at solar minimum). Aerogels could isolate the biological effects of GCR's and attenuate 1.0 - 5.0 MeV in alpha particles, but will require additional resources, nanomaterials, and insulation to shield cosmic rays, solar wind, and small impactors.

NASA has investigated GCR active and passive shielding materials including: (i) Carbon nano-materials with adsorbed H • (ii) Metal hydrides: LiH, MgH<sub>2</sub>, LiBH<sub>4</sub>, NaBH<sub>4</sub>, BeH<sub>2</sub>, TiH<sub>2</sub> and ZrH<sub>2</sub>, (iii) Pd (and alloys) with adsorbed H, (iv) Hydrocarbons (polyethylene or (CH<sub>2</sub>)<sub>n</sub>) with boron, and (v) Quasi-crystals (TiZrNi) [10]. Multilayer cosmic-ray shielding with ultralight multifunctional materials, including metallic microlattice, aerographite, and aerogels containing or filled with hydrogen. Aerographite is the lightest, and all of them are capable of holding a high volume of hydrogen, up to 99% of total weight. Aerographite is produced via single-step chemical vapor deposition (CVD) and synthesized by growing porous carbon nanotubes around a sacrificial template made from mixing and heating Zn and polyvinyl butyral powders at 900 °C [11]. Ten layers of 10-cm thick aerographite, results in a 1.0-m-thick protective layer around the entire habitat and would weigh only 113 kg. Whereas heavy materials such as lead or depleted uranium absorb all alpha, beta, gamma radiation, materials with low atomic numbers (low-Z) and hydrogen rich materials are ideal materials for radiation shielding because they do not easily break down to form secondary radiation sources. Hydrogen filled GCR multilayer insulation composed of microlattice, aerographite, and aerogel could reduce the dose equivalency of GCR to small values, 5–10 cSv /yr (50-100 mSv /year) on the surface of Mars.[12] Multilayer Cosmic-Ray Shielding design holds the potential to yield a 56-78% reduction in average radiation on Martian surface. Although a GCR dose of 50 mSv/year is bearable, it is still significantly greater than the 3 to 4 millisieverts (mSv) of radiation a year on Earth's surface. Therefore, improvements in radiation shielding material science, coatings, and nanoparticles may further reduce the dose equivalent radiation.

### 1.4 Improving Aerogel Mechanical Properties.

A 2018 study from Ma et al. used the finite volume method (FVM) to develop and analyse the stress strain curve of the SiO<sub>2</sub> aerogel and simulate compression behavior, elastic modulus and yield stress.[13] Scanning electron microscopy (SEM) and Brunauer Emmett Teller (BET) analysis were used to derive the geometrical properties of silica aerogel such as pore size, ligament diameter, and particle size. The overall elastic modulus and Poisson's ratio are obtained under an overall linear compression strain of  $5 \times 10^{-3}$ . The compressive experiment shows that the elastic modulus  $E_0$  is 0.042 GPa and the compressive yield stress  $\sigma_0$  is 0.023 GPa. SiO<sub>2</sub> aerogel studied has a tensile strain (deformation or elongation of a solid body) of 5%, 35% and 65% for the linear elastic, plastic yielding and densification, respectively.

The mechanical properties of aerogels may be described by two parameters, Young's modulus (E) and Poisson's ratio ( $\nu$ ), which is highlighted in Equation 1. The absolute value of the ratio between the longitudinal strain and transverse strain is called Poisson's ratio, which is expressed as follows:

$$V = \left| \frac{\epsilon_2}{\epsilon_1} \right| \quad \text{Eq (1)}$$

$V$  : Poisson's ratio

$\epsilon_1$  : Longitudinal strain  $\frac{\Delta L}{L}$  or  $-\frac{\Delta L}{L}$

$\epsilon_2$ : Transverse strain  $-\frac{\Delta D}{D}$  or  $\frac{\Delta D}{D}$

The compression or Bulk modulus (k), determined from Eq X, measures the stiffness of the material or the ability of the material to withstand changes in length when subjected to compressive loads, where (P) pressure and (V) is initial volume of the substance.

$$k = -V \frac{dP}{dV} \quad \text{Eq (2)}$$

The mechanical properties (elastic modulus E and yield stress  $\sigma$ ) have a power-law dependence on the relative density  $\rho$  [14,15] where m and n both represent constant as highlighted below:

$$E \propto \rho^m \quad \text{Eq (3)}$$

$$\sigma \propto \rho^n \quad \text{Eq (4)}$$

Studies detailing the scaling of mechanical properties with the density of aerogels were put forth by Fricke and Pekala et al. [16] Young's modulus (G) was found to scale with bulk density (Fb) in a power law relationship,  $G \sim Fb^a$ , where the exponent, a value varying two and four [17]. Gelation, aging, and shrinkage all play roles in defining the final mechanical properties of aerogels.

The R-value, Lankford coefficient, or Plastic Strain Ratio is the resistance of a material to thinning or thickening when put in tension or compression. The Plastic Strain Ratio can be determined using Equation 5 below where in-plane plastic strain (deformation) in numerator and plastic strain through the thickness in denominator.

$$r = \frac{\epsilon_w}{\epsilon_t} \quad \text{Eq (5)}$$

$$\epsilon_w = \ln\left(\frac{\text{width}_f}{\text{width}_o}\right)$$

$$\epsilon_t = \ln\left(\frac{\text{thickness}_f}{\text{thickness}_o}\right)$$

Copolymerization or cogellation of silanes with an organic polymer can improve mechanical aerogel reinforcement. Polydimethylsiloxane (PDMS) or aeromosils were synthesized with TEOS to demonstrate a 4-fold increase in the compressive strength over TEOS-based aerogels and recovered their original shape from a state of 30% compressive strain [18]. Moreover, when the relative density of silica aerogel is moderate and fixed around .08-.12, the pore size and ligament diameter to acquire larger elastic modulus and yield strength to optimise the mechanical behavior of SiO<sub>2</sub> aerogels. When increasing the relative density to greater than 0.16, the mechanical behavior of SA becomes much greater. The tensile properties of porous aerogels are largely dependent on the particular orientations among ligaments and the length scale of ligaments. Liu et al. [19] found that the neck radius and the strength and stiffness of the particle chains are inversely related and decrease with greater ligament lengths. Moreover, a 2013 study from South Korea mentions the negative pressure rupturing method proposed by (Kieffer and Angell 1988) can improve the porous structure and improve stability when density of SiO<sub>2</sub> aerogel is above 0.8g/cm<sup>3</sup>.

Most aerogels experience compressive and bending stresses and small strains less than 25%, which suggests the flexibility of aerogel becomes critical in such applications. A 2011 ACS study highlights leading methods to improve the Mechanical Properties of Aerogels for Aerospace Applications[20]. As the use of organo-silanes hold great promise to improve mechanical SA properties, aerogels can be strengthened by reacting the hydroxyl groups

on the silica gel surface with organic moieties carrying isocyanate groups (-NCO), followed by supercritical fluid extraction after exchanging CO<sub>2</sub> solvent. [21] With a coating of polymer on the silica aerogel backbone, the resultant aerogels demonstrate large increases in mechanical strength compared to unreinforced silica aerogels when evaluated by three point bending tests. For example, the isocyanate-reinforced aerogels supported stresses up to 800 kPa in a three-point bending test, compared to 20 kPa for a native aerogel of the same density of 280 mg/cm<sup>3</sup> [20].

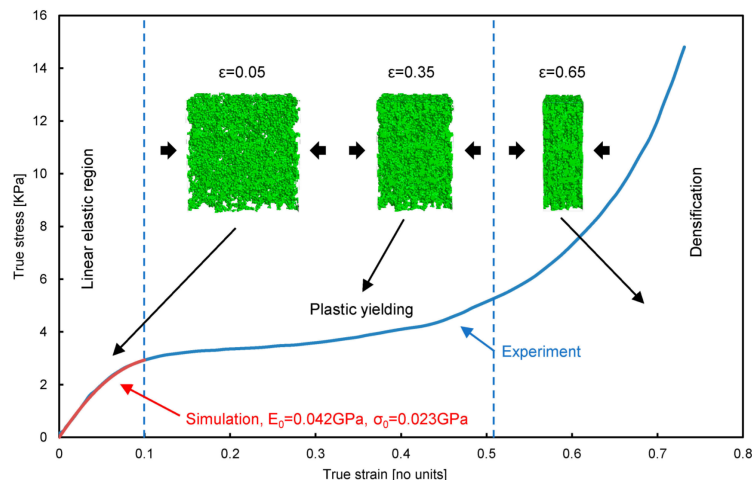


Figure 1. Stress-strain curve for a silica aerogel under compressive deformation [20].

18-25 repeat units of polymer produced the largest enhancement in mechanical properties at lower densities than previously reported.[22] The thermal conductivity of optimized aerogels varied from 19 to 36 mW/(m K) as characterized using laser flash method.

It should be noted that the ambient humidity present during testing can also alter the mechanical properties of silica aerogels, especially for hydrophilic aerogels. [20] Ambient humidity has less of an effect on mechanical properties of hydrophobic aerogels. Miner et al.[23] noted a 60% increase in Young's modulus, from 0.5 to 0.8 MPa, and a 10% increase in mass of hydrophilic silica aerogels due to water vapor uptake. As insulations may degrade due to moisture absorption or condensation when they are exposed to humidity, a 2004 study from UVA evaluated the effects of ambient humidity on the mechanical properties on hygroscopic SA. Hygroscopic aerogels were tested in a controlled humidity chamber to study the effects of adsorption of H<sub>2</sub>O in gel on Young's modulus and non-recoverable strain. Results indicate that at 70% relative humidity, the samples failed and several absorption lines indicative of hydrogen bonding between water and silica were seen to increase with increasing humidity.

A 2013 study reviews the literature on several methods to improve SiO<sub>2</sub> aerogel synthesis and mechanical reinforcing strategies [24]. Reinforcing of silica aerogels with fiber blankets inside sol before gelation is simpler and more effective when compared to the reinforcement of aerogels with separate and non-woven fibers. Reinforcing through a fiber blanket can be achieved by immersing the fiber blanket inside of the sol before gelation, facilitating large scale production [24]. Meador et al. [25] studied the use of the carbon nanofibers as reinforcement agents for polymer cross-linked aerogels. They examined the effect of incorporation of 5 wt.% carbon nanofibers in di-isocyanate cross-linked silica aerogels. In their established model, it is possible to obtain a three-fold increase in compressive modulus without any increase in density of the monoliths by increasing the fiber concentration up to 5%. And also, a five-fold increase of tensile stress at break was obtained by incorporation of 5% fiber, at lowest concentration values of total silane and cross-linker agents [25].

As the aging process can also be used to enhance mechanical SA properties, ways to expedite the aging process include heat treatment in water, [26] and soaking in alcohol [27,28] with and without additional TEOS. These processes increased the elastic modulus of the final aerogel products by roughly a factor of 2. Additionally, low dielectric Polyimide Aerogels can be used as substrates for lightweight patch antennas for the transmission of electrons with minimal electrical power loss. The polyimide aerogel antennas made from DMBZ and BPDA cross linked with TAB exhibited broader bandwidth, higher gain, and lower mass than the antennas made using commercial substrates, which is very encouraging for aerospace applications [28]. Moreover, silica aerogel is a promising candidate for replacing the conventional micron-sized silica to improve the mechanical properties of

epoxy-based nanocomposites. Mechanical tests showed improvements in flexural modulus and strength by ~80% and ~40%, respectively, as compared with those of pure epoxy. Based on this study, water-glass based silica aerogel hold great promise as a low-cost filler in polymer composite. [29]

### 1.5 Silica Aerogel Precursors and Synthesis

The manufacturing process to form silica aerogels comprises two steps: the formation of a wet gel by sol-gel chemistry, and the drying of the wet gel, when the liquid within the gel is removed leaving only the linked silica network. The significant change from the liquid to the solid stage is termed the sol-gel transition. Acids or base catalysts are used to modify sol-gel reaction time at room temperatures [30,31]. The amount and type of the used catalysts play key roles in the microstructural, physical and optical properties of the final aerogel product. Three main routes are commonly used for drying: (1) freeze-drying, in which the solvent inside of pores needs to cross the liquid-solid then the solid-gas equilibrium curve; (2) evaporation, which implies the crossing of the liquid-gas

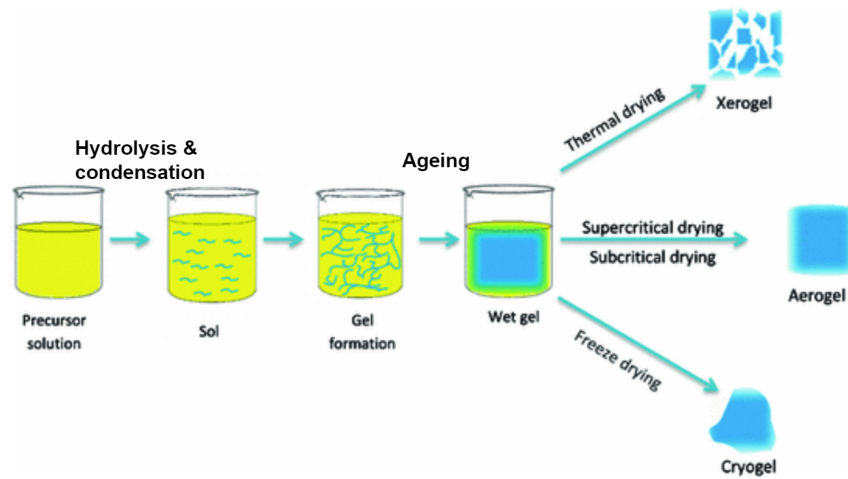
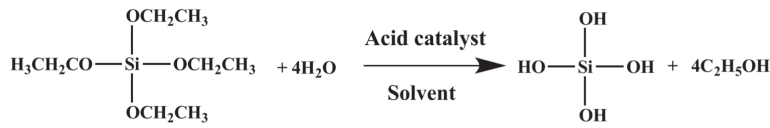


Figure 2. SA preparation and drying strategies. Source [ ]

equilibrium curve of the solvent; (3) supercritical fluids drying (SFD).

The most common of the silicon alkoxides are the tetramethyl orthosilicate (TMOS,  $\text{Si}(\text{OCH}_3)_4$ ) and tetraethylorthosilicate (TEOS,  $\text{Si}(\text{OCH}_2\text{CH}_3)_4$ ) [32], with a common chemical formula of  $\text{Si}(\text{OR})_4$ . The most common technique used for producing silica gels today involves the reaction of a silicon alkoxide with water, usually in the presence of basic, acidic, and/or fluoride-containing catalyst. The silicon alkoxide reacts with water to form silanols, which then condense to form the silica network. The key to TMOS was the use of methanol as the solvent, which was then replaced with liquid  $\text{CO}_2$  as the solvent, which alleviated the material property challenges from the supercritical drying of methanol. [34] By heating the system to 32 C, liquid  $\text{CO}_2$  can be maintained at supercritical conditions with lower pressure. The lower temperature in the drying step and nonflammability of  $\text{CO}_2$  make the process safer and less expensive.



Condensation:

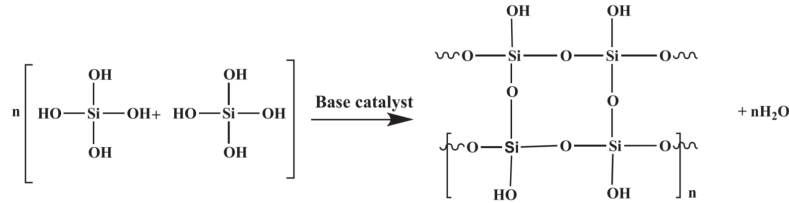


Figure 3. Silica Aerogel Synthesis with TEOS [35].

Traditional production steps and equipment to manufacture silica aerogels include: Reactors for mixing of water/alcohol and alkoxides (fluidized bed/ mechanical stirring), moulds for gelling and ageing, Methanol pools for washing and ion exchange, Supercritical drying reactor, Atmospheric CO<sub>2</sub> liquefiers and storage tanks, Methanol recycler. SA can also be obtained starting from waterglass, a substance that can be extracted from martian minerals with the use of ionic liquids. In this case, SA can be formed with the following reactions: Na<sub>2</sub>SiO<sub>3</sub>+ H<sub>2</sub>O + 2HCl → Si(OH)<sub>4</sub>+ 2NaCl.

### 1.6 Established SA Applications for Space Systems, Exploration, and Settlement

Aerogels are widely employed on Earth and find numerous applications in space as well. As previously mentioned, they are extremely successful as thermal insulators. SA is used in pipeline insulation (especially in the petrochemical and oil and gas industries) [36], cryo-insulation, buildings and constructions, windows and glasses, shipping containers and refrigeration. In construction applications, it has been shown that addition of granular aerogels to plaster and mortars leads to consistent reduction of thermal conductivity [37] [38]. Ibrahim, et al. tested the hygrothermal performance of walls with patented aerogel-based insulating rendering assessing the assembly water content, drying rate, mold growth, condensation risk, ASHRAE-160 moisture criterion, and heat losses. Results show that interior thermal insulation systems can cause several moisture problems: inability to dry out over the years, condensation risk, etc. Adding the aerogel-based rendering on the exterior surface of the un-insulated or the internally insulated walls removes or significantly reduces the moisture risks and heat losses [39]. On Earth, SA's are also used for cryogenic storage and fuel cell catalysis. In 2007, NASA developed aerogel based insulation for ambient pressure environments for liquid hydrogen (LH<sub>2</sub>) storage. Long-duration tests (up to 10 hours) showed that the potentially harmful nitrogen mass taken up inside the hydrogen storage tank is reduced by a factor of 3X for the aerogel insulated case compared to the un-insulated case [40]. In space, aerogels have been used onboard Martian rovers for thermal control and for cosmic dust collection. The aerogel structure can also be used for hypervelocity particles to gradually slow particles and capture them intact for further analysis in situ or upon EDL on Earth.

Silica aerogels can be applied to collect aerosol particles [41], to protect space mirrors, and to design tank baffles [42, 43]. Aerogels have also been used for maintaining the Seismic Experience for Interior Structure (SEIS) instrument on the NASA InSight mission to Mars. [44] Aerogels have been utilised on most Mars rovers including the Pathfinder mission, where a stable 21° C temperature was maintained in a -67° C environment. Other applications include light and efficient re-entry vehicles, heat shields, insulation of cryotanks, habitats and crew rovers, air revitalization and EVA spacesuits. However, current aerogel composites flake apart under rigorous cyclic loading-unloading tests and lose insulation quality over time. [45,46] Robust aerogel composites may also be used for baseline insulation materials of inflatable decelerators for entry, descent, and landing (EDL) vehicles [47]. ISRU production of SiO<sub>2</sub> and aerogel manufacturing facilities on Moon and Mars holds the potential to reduce launch costs, and risk of aerogel and glass fracture from launch and EDL landings. Integrating aerogel insulation and coatings into domes and greenhouses could also retain thermal heat and costs. As highlighted in the 929 pg aerogel handbook published in 2011, aerogels have also proven effective and are continuously being developed to support



containment of nuclear waste, CO<sub>2</sub> trapping, water repellent coatings, chemical sensors, heterogeneous catalysts, metal casting molds, acoustic transducers, energy storage devices, thermites, pharmaceutical drug carriers, non flammable cryogenic insulator, and confinement media to study the interactions in superfluids. [48] Aerogels are also effective materials to improve the performance of cables, dopants, pipes, plumbing, catalysts and filters, adsorption, filtration, air revitalization, rust and corrosion prevention, absorbents of heavy metal & contaminants in water, and bioengineering (antibacterial activity, wound healing, angiogenesis).

Cryogel is an insulation material used at temperatures as low as -200°C. Cryogel insulation blankets are made with a patented nanotechnology form of silica aerogel insulation with a non-woven, glass-fibre batting to strengthen the material. [49]. Developed and manufactured by Aspen Aerogels, Cryogel Z is a flexible aerogel blanket laminated to a vapor retarder with zero water vapor permeance. As highlighted in the figure below, cryogel Z has a 5-10 mm thickness with a .16g / cubic centimeter, and 116 m<sup>2</sup> roll size. With excellent acoustic and thermal protection, the aerogel blanket can be used for cryogenic pipelines, vessels and equipment, gas liquefaction & re-gasification facilities, which provide 50% less heat gain and boil off.

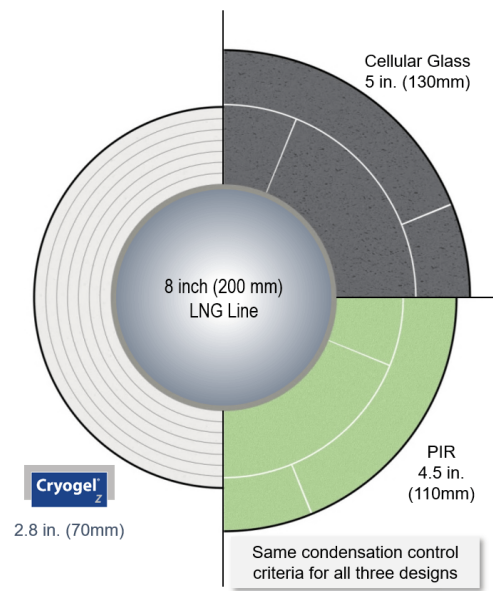


Figure 4: Cryogel Z. Source []

### 1.6 Silica Aerogel Mats for Algae Biomass Production, Water Mining, and Greenhouses

Aerogels can also provide thermal insulation on the surface of Mars and planetary bodies to maintain thermal conditions to heat soils, to melt water ice, and to sustain habitable induced greenhouses, which presents a key motivator for this SA literature review. In 2019, Wordsworth et al. [50] conducted an experiment that demonstrated a 2–3 cm-thick layer of silica aerogel will simultaneously transmit sufficient visible light for photosynthesis, block hazardous ultraviolet radiation and raise temperatures underneath it permanently to above the melting point of water, without the need for any internal heat source in Mars environment conditions. Moreover, less smoke and light could hold the potential to increase temperature into hundreds. Although, heat was lost in experimental setup via sidewall and base thermal losses and convection. Also measured transmission of aerogel particles and tiles in ultraviolet and found strong attenuation of UV-A and UV-B and near total attenuation of most hazardous UVC radiation. However, galactic cosmic rays (GCR) and higher energetic radiation particles would still penetrate through the aerogel down to around 1-meter depth. Moreover, a 2019 study demonstrated that a low scattering non-evacuated transparent aerogel could heat the environment below to intermediate temperatures (120–220 °C) and induce the greenhouse effect. The solar receiver aerogel has a scattering center diameter (which dictates optical transparency of aerogel) around 6 nm, much smaller than previously reported values of around 20 nm aerogel. Without the need for costly optical and mechanical components, the thicker aerogel layer reduces heat loss without incurring a significant optical loss, enabling a pathway to promote solar thermal energy utilisation. [51]

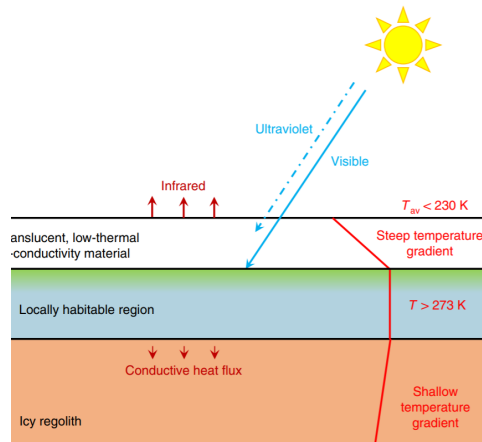


Figure 5. Effect of aerogel blankets on surface thermal environment. Source []

## 2. Silica minerals on Mars and processing techniques

### 2.1. Native Silica (SiO<sub>2</sub>) on Mars

The separation of metals from SiO<sub>2</sub> is a common process throughout the Solar System. The relatively rapid separation of silicate and iron-rich inner planets and meteorites implies both components were once both fluid (Stevenson 1990). Mars has a central core made up of metallic iron and nickel surrounded by a less dense, silicate mantle and crust. Silicon comprises around 23% on average of the Martian Crust [53], which is considered to be the second most common element on Mars, after oxygen. Pathfinder's soil samples were normalized to 44% wt of Silica for the purpose of comparison in chemical composition of Martian soil and rock analysis [53]. While silica can comprise up 90% of the composition of some of the rocks, the majority of silica is currently mixed with other elements and metal oxides. Although, there may have been geological processes that have concentrated silica into more easily usable forms.

The Figure 6 highlights NASA JPL map of Mid-latitude Martian silicon concentrations, which was

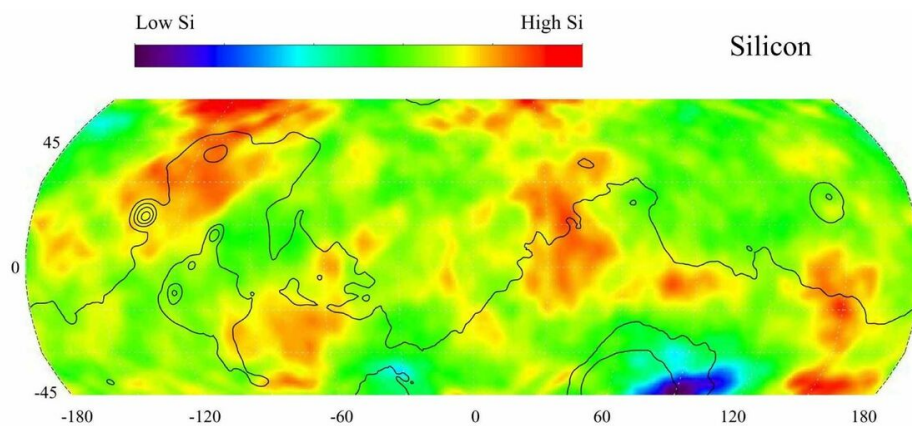


Figure 6: Mid-latitudes map of silicon concentrations on Mars. Source [].

observed from the gamma ray spectrometer onboard the 2001 Mars Odyssey orbiter. The region with the highest silicon is in the high latitudes north of Tharsis (centered near 45 degrees latitude, -120 degrees longitude) and northwest of Valles Marineris [54]. In Valles Marineris, there is evidence for a volcanic field on the floor of the deepest trough of Coprates Chasma. Spectral data reveals an opaline-silica-rich unit associated with at least one of the 130 individual structures resembling dark-colored volcanic rock scoria and tuff or volcanic ash cones that are associated with units that are interpreted as lava flows.[55] Hydrated Fe sulfates, including H<sub>3</sub>O-bearing jarosite, and are found in finely stratified deposits exposed on the floor of and on the plains surrounding the Valles Marineris.

A 2008 study on the opaline silica in young deposits on Mars, mentions the silica signatures are associated with stratigraphically lower Fe sulfates, consistent with the mineral sequence expected from evaporation of fluids produced by acidic dissolution of basalt [56]. In 1997, Mars pathfinder rover observed much higher silicon content in some of the nine rocks at Ares Vallis, Chryse Planitia compared to martian meteorites. If the high silicon-based andesites (extrusive volcanic rock) are representative of the highlands, they suggest that ancient crust on Mars is similar in composition to continental crust on Earth. This similarity would be difficult to reconcile with the very different geologic histories of the two planets. Alternatively, the rocks could represent a minor fraction of high-silicon rocks on a predominantly basaltic plain. [53] NASA's Curiosity rover has found much higher concentrations of silica at some sites it has investigated in the past seven months than anywhere else it has visited since landing on Mars 40 months ago. Multispectral data from MER Spirit rover at Gusev Crater (14.5°S 175.4°E), a 166km wide crater, near northern most part of Elysium Planitia found silica-rich deposits and hydrated minerals are bound with H<sub>2</sub>O or OH with 1009 nm pancam wavelength. Observations of the brightest exposure of soil by the rover's Alpha Particle X-Ray Spectrometer (APXS) instrument show that its composition is 90.1 wt.% SiO<sub>2</sub> (98 wt.% SiO<sub>2</sub> when corrected for dust contamination). Spectra also reveals a suite of sodium silicate minerals (magadiite (NaSi<sub>7</sub>O<sub>13</sub>(OH)<sub>34</sub>(H<sub>2</sub>O))), sodium metasilicate pentahydrate (Na<sub>2</sub>SiO<sub>3</sub>5H<sub>2</sub>O), and sodium metasilicate nonahydrate (Na<sub>2</sub>SiO<sub>3</sub>9H<sub>2</sub>O)) as geologically reasonable silica-rich material components

As SpaceX reaffirmed prioritization of Arcadia Planitia in 2019, a 2015 study from UArizona Researchers analysed the Shallow Subsurface Water Ice and minerals at two Exploration Zones (EZ) in the northern mid-latitudes of Mars in the vicinity of Arcadia and Amazonis Planitia. The uppermost surface at both of these two locations is rich in iron and silicon, 14 and 18-20 wt. % respectively, which are also of interest for ISRU. Researchers proposed a landing site centered at 192.1°E, 39.0°N near Erebus Montes and confirmed the detection of metal silicon at SROI-1 and SROI-2 [52, 57].

### 2.2.1 Hydrated Silica

There may be substantial deposits of silica gel and hydrated silica (SiO<sub>2</sub> • xH<sub>2</sub>O) within aqueously altered mineral suites and opaline mineralization by-products in hydrothermal metamorphic and weathering locations in the Martian regolith [58]. Biogenic silica (bSi), also referred to as opal, biogenic opal, or amorphous opaline silica, forms one of the most widespread biogenic minerals. bSi is hydrated silica (SiO<sub>2</sub>·nH<sub>2</sub>O), and is essential to many plants and animals. Aqueous free silica is a product of basalt weathering, when the interaction of water with mafic (i.e., Mg- and Fe-rich, silica-poor) rock rapidly dissolves olivine, pyroxene, and glass. Hydrated silica crystallinity is correlated with the geochemistry of associated minerals. Highly crystalline hydrated silica is found with Fe/Mg-phyllsilicates, moderately crystalline hydrated silica is associated with Al-phyllsilicates, and poorly crystalline phases are associated with sulfates. [59] In a 2008 study on the detection of silica-rich deposits on Mars, opaline or biogenic silica deposits (as much as 91 weight percent SiO<sub>2</sub>) have been found in association with volcanic materials by the Mars Rover Spirit [60]. The deposits are present both as light-toned soils and as bedrock and likely formed under hydrothermal conditions, which are strong indicators of a former aqueous environment.

Using near-infrared spectral data from the Compact Reconnaissance Imaging Spectrometer for Mars (CRISM) aboard the Mars Reconnaissance Orbiter (MRO), B.L. Ehlmann et al. found spatially widespread and mineralogically diverse minerals west of Isidis basin with large exposures of both mafic minerals and iron magnesium phyllosilicates in stratigraphic context. [61] Observed minerals with greater concentrations of silica can be categorised into smectite clays, phyllosilicates, felsic minerals, and mafic minerals. Mafic minerals are silicate or igneous rock rich in magnesium and iron. Most mafic minerals are dark in color, and common rock-forming mafic minerals include Olivine (Mg,Fe)<sub>2</sub>SiO<sub>4</sub>, Pyroxene (XY(Si,Al)<sub>2</sub>O<sub>6</sub>), Augite ((Ca,Na)(Mg,Fe,Al)(Si,Al)<sub>2</sub>O<sub>6</sub>), Pigeonite ((Ca,Mg,Fe)(Mg,Fe)Si<sub>2</sub>O<sub>6</sub>). Phyllosilicates, or parallel sheets of silicate tetrahedra include: Kaolinite (Al<sub>2</sub>Si<sub>2</sub>O<sub>5</sub>(OH)<sub>4</sub>}, Montmorillonite ((Na,Ca)<sub>0.33</sub>(Al,Mg)<sub>2</sub>(Si<sub>4</sub>O<sub>10</sub>)(OH)<sub>2</sub>·nH<sub>2</sub>O), micas such paragonite NaAl<sub>2</sub>[(OH)<sub>2</sub>AlSi<sub>3</sub>O<sub>10</sub>], margarite (CaAl<sub>2</sub>(Al<sub>2</sub>Si<sub>2</sub>)O<sub>10</sub>(OH)<sub>2</sub>), and Serpentine ((Mg,Fe)<sub>3</sub>Si<sub>2</sub>O<sub>5</sub>(OH)<sub>4</sub>). Felsic minerals are usually light in color rich in Quartz (SiO<sub>2</sub>), Feldspar (KAlSi<sub>3</sub>O<sub>8</sub> – NaAlSi<sub>3</sub>O<sub>8</sub> – CaAl<sub>2</sub>Si<sub>2</sub>O<sub>8</sub>), and Maskelynite.

The presence of phyllosilicates on Mars has been previously suggested on the basis of *in situ* elemental analyses by the Viking Landers 4. An unambiguous detection of water-bearing phyllosilicates has been reported over large areas [62]. The detection of phyllosilicates in small areas of Arabia Terra and northern Terra Meridiani suggests that the alteration processes could have been intense over this entire region. [63] The identification of hydrated silicate is first based on the detection of the 1.9-µm absorption band, calculated using spectral channels at 1.93 µm for the band centre and at 1.86 and 2.14 µm for the continuum. A major outcome of the present work is that phyllosilicates are detected in only a very restricted number of areas, commonly in association with two types of terrains: dark deposits and eroded outcrops. phyllosilicates, or sheet silicates, are an important group of minerals that includes the

micas, chlorite, serpentine, talc, and the clay minerals. Most phyllosilicates contain hydroxyl ion, OH<sup>-</sup>, with the OH located at the center of the 6 membered rings, as shown here. Thus, the group becomes Si<sub>2</sub>O<sub>5</sub>(OH)<sup>-3</sup>.

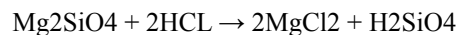
Satellite imagery of Mars surface indicates primarily mafic rock with limited patches of light-colored rock containing feldspar and quartz. Geochemical data and images of 22 specimens analysed by the Curiosity rover suggest the rocks belong to two distinct geochemical types: alkaline compositions containing up to 67 wt% SiO<sub>2</sub> and 14 wt% total alkalis (Na<sub>2</sub>O + K<sub>2</sub>O) with fine-grained to porphyritic textures on the one hand, and coarser-grained textures consistent with quartz diorite and granodiorite. Silica-rich magmatic rocks may constitute a significant fraction of ancient Martian crust and may be analogous to the earliest continental crust on Earth. [64]

In addition to warming, fracturing, and materials brought to the surface, the meteor impactors also imply a certain amount of glassification. These newly formed glasses, along with the likely presence of greater hydrogen ions in the subsurface water, are likely to produce varying quantities of silica gel. The amount of gel produced would be dependent on the amount of silica, the amount and degree of alkalinity of the subsurface water, and the temperature of the materials under-going the Alkali-Silica Reaction (ASR). ASR is a simple acid-base reaction between calcium hydroxide or Ca(OH)<sub>2</sub>, and silicic acid (H<sub>4</sub>SiO<sub>4</sub> or Si(OH)<sub>4</sub>). If the bi-products of ASR are widespread on Mars, ASR may have been significant in the weathering and erosion process. ASR reaction will tend to take place in similar conditions as life; warm, wet conditions. This similarity may make ASR Gels and products a good place to find evidence of life. [58]

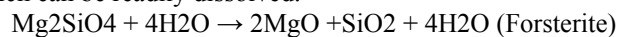
High spatial and spectral resolution reflectance data acquired by the Mars Reconnaissance Orbiter Compact Reconnaissance Imaging Spectrometer Mars (CRISM) instrument reveal the presence of H<sub>2</sub>O- and SiOH-bearing phases on the Martian surface. The spectra are most consistent with opaline silica and glass altered to various degrees. Acid-sulfate steam condensates produced by fumaroles have the capacity to leach metal cations from basaltic rocks, leaving behind a residue of opaline silica. [65] Knowing the types of opal is important, as different types may indicate different aqueous environments on Mars. Vivian Z. Sun and her colleagues distinguished between opal-A and more crystalline-hydrated silica on Mars by comparing CRISM spectral data over opal silica deposits with laboratory measurements. They found that opal-A is mostly associated with bedrock, whereas more crystalline-hydrated silica is mostly associated with aeolian sediment. Opal-A occurrences on Mars are commonly associated with bedrock exposures, whereas more crystalline hydrated silica (opal-CT and quartz/chalcedony) is primarily observed in unconsolidated sediments. [66]

### 2.3 ISRU: Mining, Extracting, and Processing Silica and Precursors from Regolith

On Earth, silica is generally not pure when mined and tends to be associated with iron hydroxide and oxy-hydroxide impurities which lowers its industrial value and requires purification before use. With high concentrations of silicon dioxide in the Martian regolith, SiO<sub>2</sub> could be extracted, processed, and stored locally nearby the settlement and production facilities. As silicon in minerals is typically highly concentrated, it still needs to undergo a separation and costly and energy-intensive purification process before industrial use. Considering SiO<sub>2</sub> is bound to several other mineral constituents and rocks on the surface of Mars, most mineral extraction and processing is likely to amass feedstocks of SiO<sub>2</sub> mixed with minerals, unpurified, and purified silica. If silicate minerals are cleaned without impurities, the cost of mineral extraction drops considerably. Traditionally, silicon rock is melted in a furnace at 4,000° F and the silicon purified even further, similar to the steel production process, which is why this molten rock is often referred to as metallurgical silicon. Silicon dioxide can also be melted and chemically transformed to manufacture glass. Before glass production, SiO<sub>2</sub> can be heated in the presence of H<sub>2</sub> in a cyclonic mixer and passed through a magnetic separator to remove any remaining iron oxide. Silica production for glass has an embodied energy of 6-15 MJ/kg. Dust collectors and atmospheric treatment systems will also be advantageous in production areas. Moreover, forsterite (Mg<sub>2</sub>SiO<sub>4</sub>), a common olivine mineral on Mars and the Moon can be treated directly with hydrochloric acid to yield silicic acid and MgCl<sub>2</sub>, accordingly:



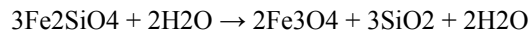
Silica may be precipitated from silicic acid yielding four moles of water. Magnesium oxide (MgO) powder may also be extracted from olivine which can be readily dissolved:



The weathering of olivine in H<sub>2</sub>O in the presence of CO<sub>2</sub> gas yields serpentine and magnetite:



The olivine fayalite (Fe, Mg)<sub>2</sub>SiO<sub>4</sub>, can be used as refractory sands, abrasives, gemstones and as mineral specimens and undergoes the following weathering reaction with H<sub>2</sub>O to also yield magnetite and silica:



### 2.3.1 SiO<sub>2</sub> Separation and Purification.

NASA Marshall Space Flight Center (MSFC) investigated using sodium silicate as a potential binder for martian regolith grains for additive construction. Metal silicates and sodium can be extracted from sodium silicate Na<sub>2</sub>SiO<sub>3</sub>, which has been observed in Martian regolith, with ionic liquids (ILs), which are organic salts that are liquid at or near room temperature. [68] For physical separation 5 kg raw sand samples were dried in the sun to remove moisture. Separation of heavy, medium and light minerals was carried out depending on specific gravity or density of the minerals using laboratory shaking tables. After the gravity separation and drying, the light fractions of Padma River sand was run into the high intensity roll magnetic separator to separate the magnetic and nonmagnetic fractions. The samples were separated at 60 rpm (magnetic fraction) and 140 rpm (paramagnetic fraction) speed by High Intensity Rolling Magnetic separator (HIRMS). The nonmagnetic part was separated again by Induced Roller Magnetic Separation (IRMS) for high precision. The remaining light fraction was separated into ferromagnetic, paramagnetic and nonmagnetic fractions with an Induced Roll Magnetic Separator (IRMS) run at 0.3 A (2000 Gauss) and 3.0 A (20 000 Gauss). This separation was done to remove feldspar and other aluminosilicates mineral form silica sand. As silica sand is non-conductor it is easily separated by this process, electrostatic plate separator (ESPS) separates the fine conductors from coarse nonconductor rich streams. The non conductive portion obtained from the ESPS is mostly the silica. The fractions separated by the Induced Roll Magnetic Separator (IRMS) were then processed by using an electrostatic plate separator (ESPS) operating at 25 kV and a feed rate of 20 rpm to separate the conductive and nonconductive minerals. The nonconductive sand particles contain high amounts of silica. It is observed that the silicon oxide (SiO<sub>2</sub>) content is significantly degraded in the magnetic fraction and upgraded in the nonmagnetic fraction [69]. This separation was done to remove iron bearing magnetic minerals from silica sand.

Following the separation of SiO<sub>2</sub>, silicon purification methods include the smelting and secondary refining of metallurgical-grade silicon and acid leaching treatment. Other methods to refine silicon include the solvent refining, vacuum treatment, plasma refining, and electron beam treatment. Developed for a variety of materials, chemical and metallurgical processes, a fluidized bed reactor (FBR) is currently used for silane pyrolysis to heat Si particles. FBR's provide lower energy consumption at around 600-650° C at lower costs and high efficiencies for uniform particle mixing, temperature gradients, and continuous operations. [70]

SiO<sub>2</sub> can also be purified via organic or polymer-based reduction as highlighted from the following four steps: (1), placing a certain amount of silicon dioxide treated with organic matter or superpolymer and sulfur in a quartz tube, feeding chlorine gas carried by nitrogen for 2 to 4 hours under 600 to 1100° C, absorbing tail gas with lime water, and cooling to 100 to 200° C; (2), pouring the cooled silicon dioxide to 5-10% hydrochloric acid, stirring fully, washing the mixture with deionized water until the mixture is neutral, and baking to obtain purified silicon dioxide. The method provided by the invention is simple in process and mild in condition and is applicable to industrialized production; silicon dioxide purified through the method can meet actual requirements on production of special quartz glass products for semiconductors and the photovoltaic industry. [71] The purified silicon can later be used as a precursor for silanol (SiH<sub>4</sub>O) and aerogel synthesis.

### 2.3.2 Carbothermal Reduction Reactors

In order to separate SiO<sub>2</sub> into constituent silicon, multipurpose carbothermal reduction reactors (CRR) can also be used to reduce metal oxides (primarily SiO<sub>2</sub>) with carbon as the reducing agent at temperatures of several hundred degrees Celsius. In 2009, NASA developed a carbothermal reduction process for usage on the Moon, where methane is used as a source of carbon, and concentrated solar energy or a laser beam is used as a heat source [72]. This process also works for silicon. As highlighted in Figure 7, a carbothermal reactor can be used to convert regolith through which methane flows continuously over the molten regolith zone. The extraction of gaseous oxygen from the oxides by reduction using hydrogen (Taylor and Carrier, 1992), molten salt electrolysis (Tripuraneni-Kilby et al., 2006) and carbothermal processing of regolith (ORBITEC, 2006) are currently being pursued by NASA (Sanders, Larson and Sacksteder, 2007). Carbothermic Reduction of Silica in an Arc Furnace has been implemented at large scales by Dow Corning, US-based conglomerate that manufactures hyperpure polycrystalline silicon to produce materials. Improvements in purity levels and large scale metallurgical reactions have been obtained in continued developments by Elkem-Exxon, Solarex, and Elkem [73]. In 2020, researchers from South Korea published a study on the ultrafast carbothermal reduction of silica to silicon using a CO<sub>2</sub> laser beam. Carbothermal

reduction took place within a few seconds of the laser beam illuminating the silica/carbon mixture. Laser beam supplied heat energy to the mixture of silica and carbon black at an intensity above  $\sim 4.29 \times 10^6 \text{ W/m}^2$ . The intensity of the laser beam and  $\text{N}_2$  gas flow during the process were critical to obtaining silicon [74]. By utilising local abundant  $\text{CO}_2$ , CRR's provide a low-mass, low power method with several advantages over existing systems to yield high purity silicon for  $\text{SiO}_2$  aerogel synthesis.

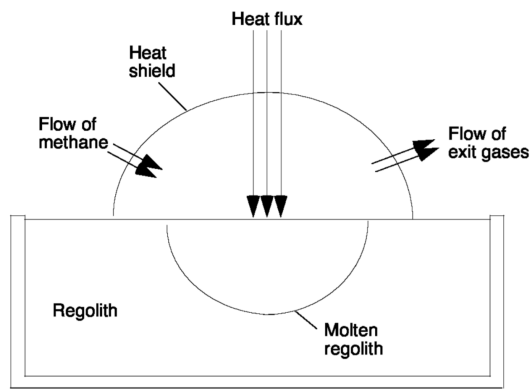


Figure 7. Schematic representation of a CRR. Source []

### 2.3.3 Microwave Regolith Processing

Alternatively, microwave processing is also a prime candidate for regolith processing of rocks, metals, silica sand, and ceramics [75,76,77,78,79,80,81,82]. Susceptor-assisted microwave heating [83] utilises a susceptor to absorb electromagnetic energy and convert it to passively heat and activate silicon dopants [84]. The susceptor-assisted microwave approach yields the advantage of becoming more independent of the regolith composition and universally applicable. Variations in iron oxide content influences processing time or processing temperature. However, there are typically greater energy requirements and thermal losses from susceptor-assisted heating than regular microwave heating. A microwave kiln was utilised in combination with a commercially available 2.5 GHz microwave oven with a maximum operating power of 1 kW. Microwaves hit the susceptor material which then starts radiating infrared heat. Since microwave processing of material occurs at high temperatures ( $> 1100 \text{ }^\circ\text{C}$ ), high-temperature materials like carbon or silicon carbide [85, 86] can be used as crucibles, both of which are also excellent susceptor materials for heating. [87]

## 2.4 Industrial Silica Life Cycle and Applications

Silica has many uses and is extensively utilised in the steel industry. Silica is the starting material for the production of ceramics and silicate glasses and is often used with molds and cores to make metal castings. Silica is also used for refractory bricks and ramming masses used in steel plants, foundries, and cement plants. Silica is also a common building material used with concrete, grout, and plaster. Abrasive blasting or sandblasting uses compressed air or water to direct a high velocity stream of an abrasive material to clean an object or surface, remove burrs, apply a texture or prepare a surface for painting.

## 2.5 Biological Silica Life Cycle on Earth

The biological silica life cycle on Earth provides a novel analog biosphere to emulate on Mars and other planetary bodies. As the primary silica reservoir is from silicate rocks in Earth's crust, silicic acid ( $\text{H}_4\text{O}_4\text{Si}$ ) is delivered to the ocean through six pathways as illustrated in the diagram, which all derive from the weathering of the Earth's crust.[88] Marine biological production of biogenic opaline silica primarily comes from diatoms [89], unicellular photosynthesising algae found in almost every aquatic environment including fresh and marine waters, soils, in fact almost anywhere moist. The major sink of the terrestrial silica cycle is exported to the ocean by rivers. Silica that is stored in plant matter or dissolved can be exported to the ocean by rivers. The rate of this transport is approximately  $6 \text{ Tmol Si yr}^{-1}$ . [90] Moreover, plants assimilate Si as soluble monosilicic acid resulting in strengthening of the cell wall through various mechanisms [91; 92]. Higher accumulation of silicon improves plant resistance to diseases, insect attack, and adverse climatic conditions in various plant species like rice, oat, barley, wheat, cucumber, and sugarcane [93, 94, 95, 96], which is favorable for crops grown in silica rich basalts around 40-50% wt  $\text{SiO}_2$  on the Moon and up to 60% wt on Martian regolith.

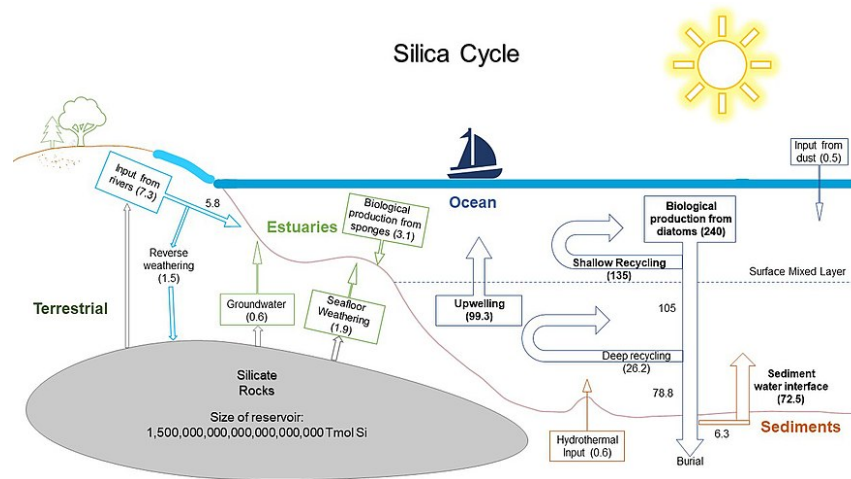


Figure 8. Schematic representation of silica cycle on Earth. Source [ ]

## 2.5 Bacteria and Algae to Biomine and Purify Silica and Silicon

On Earth, a variety of organisms utilise silica as a building material, including hexactinellid sponges, radiolarians, and diatom phytoplankton [97,98]. Diatoms have a silica rich, hard cell wall (frustule), composed almost purely of silica, made from silicic acid, coated with a layer of organic substance known as pectin. As diatoms account for around 40% of all marine carbon sequestration, diatoms store more CO<sub>2</sub> from the atmosphere than all the world's rain forests put together and produce 20% of all oxygen in the atmosphere. Biogenic silica production in the photic sunlight zone is estimated to be 240 ± 40 Tmol Si year<sup>-1</sup>. [88] Dissolution in the surface removes roughly 135 Tmol Si year<sup>-1</sup>, while the remaining Si is exported to the deep ocean within sinking particles. [90] Diatoms are primarily between 20-200 microns in diameter, and occasionally 2 millimeters in length. The diatomic near pure silica cell wall may discourage ingestion by grazing organisms, provide necessary support for the large vacuole, buoyancy for cells to access nutrient and light enriched surfaces [99] facilitate light harvesting, increase nutrient uptake, and protect the cell against UV radiation. A 2019 study on silicified cell walls in diatoms found that a 6X increase in silica content leads to a 4X decrease in copepod grazing suggesting thickening of silica walls is an effective defence strategy against being consumed by copepods. Hence, silica deposition in diatoms decreases with increasing growth rates, suggesting a possible cost of defence. [100] The silicon accumulation gene enables organisms to absorb and store silicon and is found in many algae species including cyanobacteria. As diatoms uptake and sense silicic acid from seawater via silicon transporter (SIT) proteins, a 2016 study evaluated the SIT gene family to identify potential genetic adaptations that enable diatoms to thrive in the modern ocean [101, 102] Diatoms are known to have high potential for bionanotech applications such as such as gel filtration (purification of proteins), biosensors, immunoisolation bioencapsulation, microfabrication (fibriles, tubules, nano drug delivery, lithographic masks [103]. Biomolecules such as proteins, enzymes or antibodies can be encapsulated within the silica matrix to form hybrid biosensors and bioreactors. Diatom frustules can be utilised as 3D hierarchically structured materials for photonic devices or microfluidics. [104] Diatoms such as *Phaeodactylum tricornutum* species are also ideal candidates for microbial cell factors and biomanufacturing bulk commodity products (biomass, biodiesel, protein and bioplastics) and specialty chemicals (eicosapentaenoic acid, docosahexaenoic acid, fucoxanthin and recombinant proteins, e.g., recombinant antibodies) while enabling carbon sequestration [105, 106].

Some suggest fertilising oceans with iron could promote diatom production or blooms that extract CO<sub>2</sub> out of the air. In 2004, Smetacek et al. dissolved seven metric tons of iron sulfate in acidic seawater and spewed the solution into the ship's propeller wash, which is the equivalent of adding 0.01 gram of iron per square meter. *Haetoceros atlanticus*, *Corethron pennatum*, *Thalassiothrix antarcticus* and nine other species of diatoms grew in abundance down to depth of 100 metres and carbon fell 34 times as fast as natural rates for nearly two weeks. The geoengineering approach holds the potential to sequester one billion tons of CO<sub>2</sub> per year to the ocean floor for a few centuries on Earth. As dissolved iron oxide would be more readily bioavailable in water ice melted aquatic environments on Mars, a similar particle dispersion approach to distribute other minerals could aid the growth of diatoms, algae, and aquatic organisms [107].

Radiolarians are also silica-secreting, single-celled organisms that dwell in open-ocean with a diameter of 0.1–0.2 mm, orders of magnitude larger than diatoms, and a skeleton composed of silica. On Earth, they occur throughout the water column from near the surface to great depths. Some surface-dwelling radiolarians also have algal symbionts. Silica-forming sponges also contain a silica glass skeleton such as the marine sponge, hexactinellid sponge *Euplectella* sp, that filters bacteria and plankton from the surrounding water to provide important habitats for marine life. The Venus' flower basket siliceous sponge utilises silicatein to extract silicic acid from surrounding seawater, which is then converted into complex 3D silica structures at ambient temperatures underwater [108]. While sponges catalyze silica using a specific enzyme known as silicatein, diatoms do not use silicateins but rather small specialised peptides called silaffins which attach long chain polyamines (LCPAs) to lysine groups, outlined in a study on the role of proteins in biosilicification [109]. The intracellular diatom silicification process occurs under physiological conditions at temperatures between 0 and 37°C, neutral pH, and ambient pressure, and biosilicification is around  $10^6$  times faster than the corresponding abiotic process [110], something human engineering capabilities are unable to replicate without the use of high-temperature. Thus, diatom algae could hold the potential to become a leading biomanufacturing method to extract high quality silica on planetary bodies. Further research will demonstrate the efficacy and adaptability of organisms to bioleach, to process, and to manufacture silica and silicon in-situ on Mars and beyond Earth.

Silicate solubilizing bacteria (SSB) are in soil, water, aquatic sediments and in silicate minerals on Earth and increase the bioavailability of silicates, P and K in the soil while protecting plants against pathogenic fungi. Numerous bacterial strains of genus *Bacillus*, *Pseudomonas*, *Proteus*, *Rhizobia*, *Burkholderia*, and *Enterobacter* release silicone ( $R_2SiO$ )<sub>x</sub> from silicates and promote plant growth [111, 112, 113, 114, 115, 116]. As organic acid production (gluconic, succinic, fumaric, tartaric, and maleic acid) is the most common mechanism for P and Si solubilization, the role of acidic phosphatase during Silicon solubilization has been firstly reported in a 2020 study on Silicon-Solubilization for Characterization of Bacteria and Mitigation of Biotic Stress [117]. Dominance of *Pseudomonas* and *Bacillus* spp. for the function of Si solubilization was observed during diversity analysis of Si solubilizers isolated from different rhizospheres. Functional diversity studies show genetic relatedness of *Bacillus* and *Pseudomonas* sp, a gram negative bacteria similar to extremophile cyanobacteria, a perchlorate reducer and is also capable of nitrogen fixation (e.g. strain A1501). [117] Feldspar, NBRISN13 plant bacteria, and other unexplored methods also have combinatorial effect of on the immune response through (i) increased Silicon uptake, (ii) reduced disease severity, (iii) modulation of cell wall degrading and antioxidative enzyme activities, and (iv) induced defense responsive gene expression. Moreover, 16S rRNA gene sequencing demonstrated that the Silicate solubilizing bacteria (SSB) UPMSSB7 *Enterobacter* sp showed the highest solubilization of insoluble silicate, phosphate (P) and potassium (K) at 5 and 10 days and inhibition of root diseases. [118] SSB suppressed disease and may also be used to produce silicon-solubilizing microbe based biofertilizers and nanocoatings to dissolve SiO<sub>2</sub> in aqueous environments. Bioreducing bacteria, *shewanella* strains are efficient at bioleaching silica sand and can reduce Fe(III) from silica sand. *Shewanella* strains (*S. putrefaciens* CIP8040, *S. putrefaciens* CN32, *S. oneidensis* MR-1, *S. algae* BrY and *S. loihica*) were found to remove up to 17.6% of the iron bearing impurities (~117mg of bioreducible Fe<sub>2</sub>O<sub>3</sub> per 100g of silica sand) after 15 days, and *Shewanella* algae BrY was the most efficient [119]. Growing and resting cells of *Rhodococcus erythropolis* strains PD1, R1, and FMF, and *R. qingshengii* heterotrophically removed of sulfur and bioleached iron and removed most silica impurities from coal. Results of XRF X-ray fluorescence (XRF) indicate growing cells of strain PD1 bioleached 46% of the iron and 14% of the silicate after 7 days of incubation. [120]

Algae photobioreactors hold great potential to dissolve, bioleach, and extract silicon from SiO<sub>2</sub>. A 2008 study investigated the effect of silicates with chalcopyrite (CuFeS<sub>2</sub>) and a complex multi-metal sulfide ore, on heap bioleaching in column bioreactors. Microbial inhibition and liquid flow from acid consumption, release of trace elements, and increasing the viscosity of the leach solution resulted in a negative impact of silicate mineral dissolution on heap bioleaching. Silicate minerals are present in association with metal sulfides in ores and the SiO<sub>2</sub> dissolution occurs when the sulfide minerals are bioleached in heaps for metal recovery. Algae photobioreactors provides an affordable, low power and mass method to catalyze the decomposition of ore (without grinding) such as newly mined/run-off-the-mine (ROM) materials (intermediate grade oxides and secondary sulfides). Both the artificial and biological method become avenues to in situ manufacture, process, and utilise abundant silicon on Moon and Mars, as a stepping stone to apply to other celestial bodies.



### 3. Alternatives and future perspectives

#### 3.1 Methods to Improve Performance of SiO<sub>2</sub> Aerogels

Silica aerogel demands improved mechanical and structural properties for many applications. Alternative nanomaterials can aid or replace silica-based aerogel. Polyethylene glycol (PEG), or H-(O-CH<sub>2</sub>-CH<sub>2</sub>)<sub>n</sub>-OH is found to be very effective additive, mixed during stirring process before aging, for the improvement of the mechanical properties of aerogel, which broke down at 21,924.6 N/m<sup>2</sup> with elongation of 0.8 cm. [121]. Notably, a three-fold increase in compressive modulus with 5% carbon nanofiber was observed for aerogels with a silica backbone of di-isocyanate cross-linked silica aerogels. A 5X increase of tensile stress at break is predicted by including 5% fiber when total silane and di-isocyanate concentration are low without any change in the density or porosity of the aerogels. Perhaps the great effect of including carbon fiber in the aerogels may be an improvement in the strength of the initial hydrogels before cross-linking. [122] The high surface density of silanol groups provides for easy synthesis of silica aerogel, which is particularly important in the preparation of hydrophobic hydrogels [33]. Hydrogels are crosslinked hydrophilic polymers that do not dissolve in H<sub>2</sub>O and can swell in water and hold a large amount of water. They can be formed with the following reactions:  $\text{Na}_2\text{SiO}_3 + \text{H}_2\text{O} + 2\text{HCl} \rightarrow \text{Si}(\text{OH})_4 + 2\text{NaCl}$ .

A separate 2021 study found optimal parameters of the carbon fiber-silica aerogel composite for silica aerogel reinforced with 10 vol.% of carbon fibers. [123] Thin film aerogels can also be reinforced with electrospun flexible nanofibers to bridge cracks and hold structures together before the aging and drying process [124]. A variety of nanomaterials and particles may also be fused into aerogels to help impede and potentially harvest incoming radiation. The radiation, refraction index (bending of a high energetic particle) and ability to block ionising particles could be improved by filling and compacting greater quantities of hydrogen atoms inside a porous aerogel network. An aerogel skeleton or 3D printed lattice with geometric pores could be designed to leverage the spin and collisions of hydrogen atoms. Multiscale channeled macro and mesopore networks inside aerogels could be reservoirs of nanoparticles and hydrogen-rich materials to potentially improve the radiation shielding properties. Moreover, hydrogen-rich water vapor could potentially be adsorbed from beneath SiO<sub>2</sub> aerogel to form compact hydrogen-dense structured layers to reflect radiation GCR's. Moreover, smart aerogels have recently been developed. Synthesis of shape memory aerogels by means of a shape memory polymer as reinforcement agent is a promising area of investigation. For example, a polyurethane block copolymer as a shape memory polymer can be used as a reinforcing agent for the silica aerogel network [125]. As this polymeric system is able to change its shape in response to external stimuli, the aerogels can be stored in deformed state aboard a spacecraft. [126]

#### 3.2 Cross-linked polyimide (PI) Aerogels

Aerogels can be cross linked with plastic-like polymers to form covalent bonds and to join polymer chains together and reinforce the desired material and structural properties. All polyimide (PI) nano-aerogels (polymer with repeating amide bonds) are as strong or stronger than polymer reinforced silica aerogels at the same density. By varying the structure of diamine (PPDA, ODA, BAX) and dianhydrides (BTDA and HFDA), the material properties such as flexibility, thermal oxidative stability, mechanical properties, and thermal conductivity) can be tailored to the desired application. [124] Moreover, cross linked polyimide hydrogels are 500 times stronger than silica aerogel and more flexible. NASA Glenn Research Center synthesized polyimide aerogel by cross-linking through an aromatic triamine or polyhedral oligomeric silsesquioxane. Formulations made using 4,4'-oxydianiline or 2,2'-dimethylbenzidine can be fabricated into continuous thin films using a roll to roll casting process. The 2012 study entitled Tailoring Properties of Cross-Linked Polyimide Aerogels for Better Moisture Resistance, Flexibility, and Strength, found that replacing ODA with 50 mol % of DMBZ maintains the flexibility of thin films, while the moisture resistance of the aerogels is greatly improved [18]. The films are flexible enough to be rolled or folded back on themselves and recover completely without cracking or flaking, and have tensile strengths of 4-9 MPa. As highlighted in a 2010 patent entitled Highly porous and mechanically strong ceramic oxide aerogels, polymer reinforcement doubles the density and results in two orders of magnitude increase in strength, and reduces surface area by 30-50% [127]. Another area of interest is to study the effectiveness of cage-shaped silanes available in the form of polyhedral oligomeric silsesquioxane (POSS), which cross-linking during the synthesis of flexible and foldable polyimide aerogels. [128] Polymer-reinforced silica aerogel can be streamlined to manufacture flexible thin sheets to be wrapped around pipes, tanks or other assemblages needing insulation, or used as flexible insulation for space suits or inflatable structures [20]. Cross-linked polyimide aerogels are a viable approach to higher temperature resistant, flexible insulation for inflatable decelerators.

### 3.3 Sprayable Aerogel Nanocoatings

Sprayable aerogel nanoparticles can also be thermally sprayed to improve the deposition, placement, time duration, and installation process. The insulation structure includes aerogel agglomerates formed by combining ceramic particles with aerogel particles. The method for forming an insulation structure includes spray-drying and post-drying a mixture of ceramic particles, aerogel particles, water, and a binder. [129] Researchers from China developed a novel Frozen Spray-Coating method to prepare a graphene aerogel (GA) sponge mat with enhanced mechanical, and electrochemical properties. GA mat has prominent potential in the fields of pollution absorption, supercapacitors, battery electrodes, and electromagnetic shielding. [130] Danny Ou, et al elaborate in a 2013 study on a sprayable aerogel insulation with silica aerogel beads yields a great mechanical integrity and provides lower thermal conductivity than incumbent polyurethane spray-on foam insulation, at similar or lower areal densities, to prevent insulation cracking and debonding in an effort to eliminate the generation of inflight debris. Silica aerogel beads with a packing density of 0.03 to 0.05 g/cm<sup>3</sup> were added in a mixture with binders or foams to form complex shapes, or sprayed onto panels. The aerogel compositions can withstand repeated cycles of high enthalpy shear flows of 20 to 100 Pa at temperatures tested up to 370 °C without losing mechanical integrity. The aerogel bead bindersprayed panel, with a thermal conductivity of 20 to 25 mW/mK, outperformed the commercial foam by 30 to 40 percent in the 10 to 100 °C temperature range. Compression modulus for the aerogel bead/foam composite was 60 percent higher than the one from the foam without aerogel dopant. The sprayable insulation can be utilised in various thermal management systems that require low mass and volume, such as cryogenic storage tanks, pipelines, space platforms, and launch vehicles. [131]

### 3.4 Future Research to Advance Silica Life Cycle, Aerogels, Coatings, Nanoparticles

A 3-cm thick layer aerogels sheet, or cyanobacteria algae roof, holds the potential to transmit sufficient visible light for photosynthesis, block hazardous ultraviolet radiation and induce greenhouse effect to create habitable aqueous environments on the surface of Mars and planetary bodies without the need for any internal heat source. Future research with Mars University will focus on the design, engineering, and experiments of SiO<sub>2</sub> shields for algae biomass production, water ice mining, and greenhouses. Research may prioritize the deposition of heat-responsive microcapsules loaded with polymerized organosiloxane as a novel technique to anchor SiO<sub>2</sub> aerogel sheets to regolith and other methods to reduce losses from convection and sidewall and base conduction. Novel methods and experiments in analog environments will guide the development of sprayable SA nanocoating, aerogel material testing in Mars Environment chamber, detailed modeling of microfluidics, and microbial interactions in aqueous habitable environment underneath SiO<sub>2</sub> aerogel. Moreover, carbon nanotubes are probably the next most efficient GCR shielding element after hydrogen. Nano-carbons storage of large amounts of hydrogen seems well-documented at 6% wt and claims of up to and exceeding 20% have been published [132]. Further research may focus on novel methods to synthesize, etch, and increase the radiation refractive ability with hydrogen in SiO<sub>2</sub> aerogels. Additionally, diatoms evolving in marine environments at greater depths and freezing waters provide analog organisms and environments to observe effects of limited or no sunlight on diatom growth, which could unlock clues to the biological mechanisms to mimic or adapt photosynthetic algae to the 44% solar irradiance on Mars surface. In addition to evaluating diatom microbial cell factories and algal photobioreactors, research may emphasize the efficacy, genes, bioengineering pathways, effects of %Gs, and modeling of diatom algae species as Mars microbial candidates.

## References

- [1] Solimani, Ali & Abbasi, M. (2008). Silica Aerogel; Synthesis, Properties and Characterization. *Journal of Materials Processing Technology*, 199, 10-26. <http://dx.doi.org/10.1016/j.jmatprotec.2007.10.060>
- [2] Lide, D. R., ed. (2005). *Thermal conductivity in CRC Handbook of Chemistry and Physics* (86th ed.). Boca Raton (FL): CRC Press. ISBN 0-8493-0486-5. Section 12, p. 227
- [3] David Tetlow and Theo Elmer, The state of the art: Superinsulation construction materials under the UK's domestic energy building: Aerogel and vacuum insulation technology applications, 14th International Conference on Sustainable Energy Technologies – SET 2015.
- [4] Saffa B. Riffat, Guoquan Qiu, A review of state-of-the-art aerogel applications in buildings, *International Journal of Low-Carbon Technologies*, Volume 8, Issue 1, March 2013, Pages 1–6. <https://doi.org/10.1093/ijlct/cts001>
- [5] Woignier T, Primera J, Alaoui A, Etienne P, Despestis F, Calas-Etienne S. Mechanical Properties and Brittle Behavior of Silica Aerogels. *Gels*. 2015; 1(2):256-275. <https://doi.org/10.3390/gels1020256>
- [6] Klein, L., Aparicio, M., & Jitianu, A. (2019). *Handbook of sol-gel science and technology*. Springer International Publishing.
- [7] Hassler, Donald M et al. Mars' surface radiation environment measured with the Mars Science Laboratory's Curiosity rover, *Science* (New York, N.Y.) vol. 343,6169 (2014): 1244797. <https://doi.org/10.1126/science.1244797>
- [8] [1]Reitz, G., Berger, T., and Matthiae, D., Radiation exposure in the moon environment, *Planetary and Space Science*, vol. 74, no. 1, pp. 78–83, 2012. <https://doi.org/10.1016/j.pss.2012.07.014>
- [9] Mullenders, Leon H F . Solar UV damage to cellular DNA: from mechanisms to biological effects. *Photochemical & photobiological sciences : Official journal of the European Photochemistry Association and the European Society for Photobiology* vol. 17,12 (2018): 1842-1852. <https://doi.org/10.1039/c8pp00182k>
- [10] Adams JH et al (2005) Revolutionary concepts of radiation shielding for human exploration of space. NASA TM 213688, <https://ntrs.nasa.gov/citations/20050180620>
- [11] Mecklenburg, M., et al. (2012), Aerographite: Ultra Lightweight, Flexible Nanowall, Carbon Microtube Material with Outstanding Mechanical Performance. *Adv. Mater.*, 24: 3486-3490. <https://doi.org/10.1002/adma.201200491>
- [12] Letfullin, Renat & George, Thomas & Ramazanov, Asror. (2019). Multifunctional Cosmic-Ray Shielding of Spacecraft with Elements of Systems Engineering Design. *Journal of Spacecraft and Rockets*. 56. 1-10. <http://dx.doi.org/10.2514/1.A.34440>
- [13] Ma H, Zheng X, Luo X, Yi Y, Yang F. Simulation and Analysis of Mechanical Properties of Silica Aerogels: From Rationalization to Prediction. *Materials*. 2018; 11(2):214. <https://doi.org/10.3390/ma11020214>
- [14] J Gross et al 1988 Mechanical properties of SiO<sub>2</sub> aerogels, *Journal of Physics D: Applied Physics*, Volume 21, Number 9 1447, <https://iopscience.iop.org/article/10.1088/0022-3727/21/9/020>
- [15] J Gross I, G Reichenauer I and J Fricke I, Mechanical properties of SiO<sub>2</sub> aerogels, *Journal of Physics D: Applied Physics*, Volume 21, Number 9. <http://dx.doi.org/10.1088/0022-3727/21/9/020>
- [16] Guoqing Zu, et al. Robust, Highly Thermally Stable, Core–Shell Nanostructured Metal Oxide Aerogels as High-Temperature Thermal Superinsulators, Adsorbents, and Catalysts, *Chemistry of Materials* 2014 26 (19), 5761-5772. <https://doi.org/10.1021/cm502886t>
- [17] Gen Hayase, et al, Polymethylsilsesquioxane–Cellulose Nanofiber Biocomposite Aerogels with High Thermal Insulation, Bendability, and Superhydrophobicity, *ACS Applied Materials & Interfaces* 2014 6 (12), 9466-9471, <https://doi.org/10.1021/am501822y>
- [18] Haiquan Guo, et al, Tailoring Properties of Cross-Linked Polyimide Aerogels for Better Moisture Resistance, Flexibility, and Strength, *ACS Applied Materials & Interfaces* 2012 4 (10), 5422-5429, <https://doi.org/10.1021/am301347a>
- [19] Liu, Qiang et al. Simulation of the tensile properties of silica aerogels: the effects of cluster structure and primary particle size. *Soft matter* vol. 10,33 (2014): 6266-77. <https://doi.org/10.1039/c4sm01074d>
- [20] Randall, Jason P et al. Tailoring mechanical properties of aerogels for aerospace applications. *ACS applied materials & interfaces* vol. 3,3 (2011): 613-26. <https://doi.org/10.1021/am200007n>
- [21] Thanh-Dinh Nguyen, et al., Biotemplated Lightweight  $\gamma$ -Alumina Aerogels, *Chemistry of Materials* 2018 30 (5), 1602-1609 <https://doi.org/10.1021/acs.chemmater.7b04800>
- [22] Liu, Shuo & Shah, Mihir & Rao, Satyarit & An, Lu & Mohammadi, Mohammad Moein & Kumar, Abhishek & Ren, Shenqiang & Swihart, Mark. (2021). Flame aerosol synthesis of hollow alumina nanoshells for application in thermal insulation. *Chemical Engineering Journal*. 428. 131273. <http://dx.doi.org/10.1016/j.cej.2021.131273>
- [23] Javadi, Alireza et al (2013). Polyvinyl Alcohol-Cellulose Nanofibrils-Graphene Oxide Hybrid Organic Aerogels. *ACS applied materials & interfaces*. 5. <http://dx.doi.org/10.1021/am400171y>
- [24] Maleki, Hajar & Durães, Luisa & Portugal, Antonio. (2014). An Overview on Silica Aerogels Synthesis and Different Mechanical Reinforcing Strategies. *Journal of Non-Crystalline Solids*. 385. 55–74. <http://dx.doi.org/10.1016/j.jnoncrysol.2013.10.017>
- [25] Mary Ann B. Meador et al., Reinforcing polymer cross-linked aerogels with carbon nanofibers, *Journal of Materials Chemistry*, Issue 16, 2008. <https://pubs.rsc.org/en/content/articlelanding/2008/JM/b800602d#divRelatedContent&articles>
- [26] Duan, Yannan et al. (2013). Reinforcement of Silica Aerogels Using Silane-End-Capped Polyurethanes. *Langmuir : the ACS journal of surfaces and colloids*. 29. <https://doi.org/10.1021/la4007394>
- [27] Wang, Xiao, and Sadhan C Jana. Tailoring of morphology and surface properties of syndiotactic polystyrene aerogels. *Langmuir : the ACS journal of surfaces and colloids* vol. 29,18 (2013): 5589-98. <https://doi.org/10.1021/la400492m>
- [28] Mary Ann B. et al., Low Dielectric Polyimide Aerogels As Substrates for Lightweight Patch Antennas, *ACS Applied Materials & Interfaces* 2012 4 (11), 6346-6353. <https://doi.org/10.1021/am301985s>
- [29] Salimian, S., Zadhoush, A. Water-glass based silica aerogel: unique nanostructured filler for epoxy nanocomposites. *J Porous Mater* 26, 1755–1765 (2019). <https://doi.org/10.1007/s10934-019-00757-3>
- [30] Pope, Edward J. A. and John Douglas Mackenzie. Sol-gel processing of silica. II: The role of the catalyst. *Journal of Non-crystalline Solids* 87 (1986): 185-198. [https://doi.org/10.1016/S0022-3093\(86\)80078-3](https://doi.org/10.1016/S0022-3093(86)80078-3)
- [31] Brinker, C. Jeffrey et al. Sol-gel transition in simple silicates II, *Journal of Non-crystalline Solids* 63 (1982): 45-59. [https://doi.org/10.1016/0022-3093\(84\)90385-5](https://doi.org/10.1016/0022-3093(84)90385-5)
- [32] GW, S. (1990). *Sol-gel science - the physics and chemistry of sol-gel processing*. New York, NY, Academic Press Inc.
- [33] Silica aerogel. Aerogel.org RSS. (2021). Retrieved December 31, 2021, from <http://www.aerogel.org/?p=16>
- [34] Li, Xin et al. Template-Free Self-Assembly of Fluorine-Free Hydrophobic Polyimide Aerogels with Lotus or Petal Effect. *ACS applied materials & interfaces* vol. 10,19 (2018): 16901-16910. <https://doi.org/10.1021/acsami.8b04081>

- [35] Maleki, Hajar & Durães, Luisa & Portugal, Antonio. (2014). An Overview on Silica Aerogels Synthesis and Different Mechanical Reinforcing Strategies. *Journal of Non-Crystalline Solids*. 385. 55–74. <https://doi.org/10.1016/j.inoncrsol.2013.10.017>
- [36] Coffman, B. & Fesmire, James & White, Shannon & Gould, G. & Augustynowicz, S.. (2010). Aerogel blanket insulation materials for cryogenic applications. *AIP Conference Proceedings*. 1218. 913-920. <https://doi.org/10.1063/1.3422458>
- [37] Buratti, Cinzia, Elisa Moretti, Elisa Belloni, and Fabrizio Agosti. 2014. Development of Innovative Aerogel Based Plasters: Preliminary Thermal and Acoustic Performance Evaluation, *Sustainability* 6, no. 9: 5839-5852. <https://doi.org/10.3390/su6095839>
- [38] Ng, Serena & Sandberg, Linn & Jelle, Bjørn. (2015). Insulating and Strength Properties of an Aerogel-Incorporated Mortar Based an UHPC Formulations. *Key Engineering Materials*. 629. 43-48. 10.4028/[www.scientific.net/KEM.629-630.43](http://www.scientific.net/KEM.629-630.43)
- [39] Ibrahim, Mohamad & Wurtz, Etienne & Biwole, Pascal & Achard, Patrick & Sallee, Hebert. (2014). Hygrothermal performance of exterior walls covered with aerogel-based insulating rendering. *Energy and Buildings*. 84. 241–251. <https://doi.org/10.1016/j.enbuild.2014.07.039>
- [40] Fesmire, James & Sass, Jared. (2008). Aerogel insulation applications for liquid hydrogen launch vehicle tanks. *Cryogenics*. 48. 223-231. <http://dx.doi.org/10.1016/j.cryogenics.2008.03.014>
- [41] Guise MT, Hosticka B, Earp BC, Norris PM (1995) An experimental investigation of aerosol collection utilizing packed beds of silica aerogel microspheres. *J Non-Cryst Solids* 285:317–322
- [42] Hrubesh LW (1998) Aerogel applications. *J Non-Cryst Solids* 225:335–342
- [43] Schmidt M, Schwertfeger F (1998) Applications for silica aerogel products. *J Non-Cryst Solids* 225:364–368
- [44] Petkov, Mihail & Jones, Steven & Voecks, Gerald. (2019). Zeolite-loaded aerogel as a primary vacuum sorption pump in planetary instruments. *Adsorption*. 25. <https://link.springer.com/article/10.1007/s10450-018-00003-3>
- [45] Wang, Jin, and Xuetong Zhang. Binary Crystallized Supramolecular Aerogels Derived from Host-Guest Inclusion Complexes. *ACS nano vol. 9,11* (2015): 11389-97. <https://doi.org/10.1021/acsnano.5b05281>
- [46] Maleki, Hajar & Durães, Luisa & Portugal, Antonio. (2015). Development of Mechanically Strong Ambient Pressure Dried Silica Aerogels with Optimized Propertie. *The Journal of Physical Chemistry C*. 119. 7689–7703. <http://dx.doi.org/10.1021/jp5116004>
- [47] Zu, Guoqing & Shen, Jun & Wang, Wenqin & Zou, Liping & Lian, Ya & Zhang, Zhihua. (2015). Silica-Titania Composite Aerogel Photocatalysts by Chemical Liquid Deposition of Titania onto Nanoporous Silica Scaffolds. *ACS applied materials & interfaces*. 7. <http://dx.doi.org/10.1021/am5089132>
- [48] Michel A. Aegerter, et al, *Aerogels Handbook 2011*. ISBN : 978-1-4419-7477-8, <https://link.springer.com/book/10.1007/978-1-4419-7589-8>
- [49] The INSULCON Group. Pyrogel and Cryogel insulation -200°C up to 650°C , The Insulcon Group. Retrieved December 31, 2021, from <https://www.insulcon.com/products/pyrogel-and-cryogel-products/>
- [50] Wordsworth, R., Kerber, L. & Cockell, C. Enabling Martian habitability with silica aerogel via the solid-state greenhouse effect. *Nat Astron* 3, 898–903 (2019). <https://doi.org/10.1038/s41550-019-0813-0>
- [51] Zhao, Lin et al. Harnessing Heat Beyond 200 °C from Unconcentrated Sunlight with Nonevacuated Transparent Aerogels. *ACS nano vol. 13,7* (2019): 7508-7516. <https://doi.org/10.1021/acsnano.9b02976>
- [52] D. Viola, et al., MID-LATITUDE MARTIAN ICE AS A TARGET FOR HUMAN EXPLORATION, ASTROBIOLOGY, AND IN-SITU RESOURCE UTILIZATION, First Landing Site/Exploration Zone Workshop for Human Missions to the Surface of Mars (2015), <https://www.hou.usra.edu/meetings/explorationzone2015/pdf/1011.pdf>
- [53] T., Rieder & Economou, et al. (1998). The Chemical Composition of Martian Soil and Rocks Returned by the Mobile Alpha Proton X-ray Spectrometer: Preliminary Results from the X-ray Mode. *Science (New York, N.Y.)*. 278. <http://dx.doi.org/10.1126/science.278.5344.1771>
- [54] Map of Martian Silicon at Mid-Latitudes, March 13, 2003, NASA JPL and CalTech., Retrieved from <https://www.jpl.nasa.gov/images/pia04256-map-of-martian-silicon-at-mid-latitudes>
- [55] Brož, P., Hauber, E., Wray, J. J., and Michael, G., Amazonian volcanism inside Valles Marineris on Mars, *Earth and Planetary Science Letters*, vol. 473, pp. 122–130, 2017. <https://doi.org/10.1016/j.epsl.2017.06.003>
- [56] Milliken, R.E., Swayze, G.A., Arvidson, R.E., Bishop, J.L., Clark, R.N., Ehmann, B.L., Green, R.O., Grotzinger, J.P., Morris, R.V., Murchie, S.L., Mustard, J.F., & Weitz, C.M. (2008). Opaline silica in young deposits on Mars. *Geology*, 36, 847-850. <https://doi.org/10.1130/G24967A.1>
- [57] D. Viola, et al., Arcadia Planitia: Acheron Fossae and Erebus Montes Workshop Abstract #1011, [https://www.nasa.gov/sites/default/files/atoms/files/viola\\_arcadiaplanitia\\_final\\_tagged.pdf](https://www.nasa.gov/sites/default/files/atoms/files/viola_arcadiaplanitia_final_tagged.pdf)
- [58] D. H. Graham I. and J. C. Cawley, ALKALI SILICA REACTIVITY A PROBLEM ON EARTH, A SOLUTION ON MARS, *Lunar and Planetary Science XLVIII* (2017), <https://www.hou.usra.edu/meetings/lpsc2017/pdf/2209.pdf>
- [59] Smith, Matthew & Bandfield, Joshua & Cloutis, Edward & Rice, Melissa. (2013). Hydrated silica on Mars: Combined analysis with near-infrared and thermal-infrared spectroscopy. *Icarus*. 223. 633–648. <https://doi.org/10.1016/j.icarus.2013.01.024>
- [60] Squyres, S, et al. (2008). Detection of Silica-Rich Deposits on Mars. *Science (New York, N.Y.)*. 320. 1063-7. <http://dx.doi.org/10.1126/science.1155429>
- [61] [https://www.researchgate.net/publication/251425833\\_Identification\\_of\\_hydrated\\_silicate\\_minerals\\_on\\_Mars\\_using\\_MRO-CRISM\\_Geologic\\_context\\_near\\_Nili\\_Fossae\\_and\\_implications\\_for\\_aqueous\\_alteration](https://www.researchgate.net/publication/251425833_Identification_of_hydrated_silicate_minerals_on_Mars_using_MRO-CRISM_Geologic_context_near_Nili_Fossae_and_implications_for_aqueous_alteration)
- [62] Bibring, J.-P. et al. Mars surface diversity as revealed by the OMEGA/Mars Express observations. *Science* 307, 1576–1581 (2005)
- [63] Poulet, F., Bibring, JP, Mustard, J. et al. Phyllosilicates on Mars and implications for early martian climate. *Nature* 438, 623–627 (2005). <https://doi.org/10.1038/nature04274>
- [64] Sautter, V., Toplis, M., Wiens, R. et al. In situ evidence for continental crust on early Mars. *Nature Geosci* 8, 605–609 (2015). <https://doi.org/10.1038/ngeo2474>
- [65] Ruff, S., Farmer, J. Silica deposits on Mars with features resembling hot spring biosignatures at El Tatio in Chile. *Nat Commun* 7, 13554 (2016). <https://doi.org/10.1038/ncomms13554>
- [66] Sun, V. Z., & Milliken, R. E. (2018). Distinct geologic settings of opal-A and more crystalline hydrated silica on Mars. *Geophysical Research Letters*, 45, 10,221– 10,228. <https://doi.org/10.1029/2018GL078494>
- [67] Clifford, Stephen M.. A model for the hydrologic and climatic behavior of water on Mars. *Journal of Geophysical Research* 98 (1993): 10973-11016. [https://www.lpi.usra.edu/meetings/earlymars2012/reprintLibrary/Clifford\\_1993.pdf](https://www.lpi.usra.edu/meetings/earlymars2012/reprintLibrary/Clifford_1993.pdf)
- [68] Litkenhous, Susanna (2019). Ionic Liquids, NASA Webpage, 2019 Retrieved from, <https://www.nasa.gov/oem/ionicliquids>
- [69] Rafi, A.S.M.M. & Tasnim, U.F. & Rahman, M.S.. (2018). Quantification and Qualification of Silica Sand Extracted from Padma River Sand. *IOP Conference Series: Materials Science and Engineering*. 438. 012037. <http://dx.doi.org/10.1088/1757-899X/438/1/012037>

- [70] Dudukovic, M. P., 1986, Fluidized-bed reactor modeling for production of silicon by silane pyrolysis, NASA NTSR JPL Proceedings of the Flat-Plate Solar Array Project Workshop on Low-Cost Polysilicon for Terrestrial Photovoltaic Solar-Cell Applications, Retrieved from <https://ntrs.nasa.gov/citations/19860017215>
- [71] Method for purifying silicon dioxide, Wuhan University WHU (2014). CN Patent CN103435049A <https://patents.google.com/patent/CN103435049A/en>
- [72] Balasubramaniam, R. & Hegde, U. & Gokoglu, S.. (2008). Carbothermal Processing of Lunar Regolith Using Methane. 969. 157-161. <http://dx.doi.org/10.1063/1.2844962>
- [73] Flat-Plate Solar ARray Project Final Report Volume II: Silicon Material, (1986) NASA JPL Publication 86-31, [https://www2.jpl.nasa.gov/adv\\_tech/photovol/2016PROJ/FSA%20Final%20Rpt%20II%20-%20Silicon%20Material\\_1986.pdf](https://www2.jpl.nasa.gov/adv_tech/photovol/2016PROJ/FSA%20Final%20Rpt%20II%20-%20Silicon%20Material_1986.pdf)
- [74] Maeng, SH., Lee, H., Park, M.S. et al. Ultrafast carbothermal reduction of silica to silicon using a CO<sub>2</sub> laser beam. *Sci Rep* 10, 21730 (2020). <https://doi.org/10.1038/s41598-020-78562-1>
- [75] Nekoovaght P, Gharib N, Hassani F et al (2015) The behavior of rocks when exposed to microwave radiation. In: 13th ISRM international congress of rock mechanics. International Society for Rock Mechanics
- [76] Li W, Wei J, Wang W, Hu D, Li Y, Guan J (2016) Ferrite-based metamaterial microwave absorber with absorption frequency magnetically tunable in a wide range. *Mater Des* 110:27–34. <https://doi.org/10.1016%2Fj.matdes.2016.07.118>
- [77] Batchelor A, Jones D, Plint S, Kingman S (2015) Deriving the ideal ore texture for microwave treatment of metalliferous ores. *Miner Eng* 84:116–129. <https://doi.org/10.1016%2Fj.mineng.2015.10.007>
- [78] Chandrasekaran S, Basak T, Ramanathan S (2011) Experimental and theoretical investigation on microwave melting of metals. *J Mater Process Technol* 211(3):482–487. <https://doi.org/10.1016%2Fj.jmatprotec.2010.11.001>
- [79] Liu C, Zhang L, Peng J, Srinivasakannan C, Liu B, Xia H, Zhou J, Xu L (2013) Temperature and moisture dependence of the dielectric properties of silica sand. *J Microw Power Electromagn Energy* 47(3):199–209. <https://doi.org/10.1080%2F08327823.2013.11689858>
- [80] Subasri R, Mathews T, Sreedharan O, Raghunathan V (2003) Microwave processing of sodium beta alumina. *Solid State Ionics* 158(1):199–204. <https://doi.org/10.1016%2FSS0167-2738%2802%2900772-5>
- [81] Katz JD (1992) Microwave sintering of ceramics. *Annu Rev Mater Sci* 22(1):153–170, <https://doi.org/10.1146%2Fannurev.ms.22.080192.001101>
- [82] Rao K, Ramesh P (1995) Use of microwaves for the synthesis and processing of materials. *Bull Mater Sci* 18(4):447–465, <https://doi.org/10.1007%2FBF02749773>
- [83] Bhattacharya M, Basak T (2016) A review on the susceptor assisted microwave processing of materials. *Energy* 97:306–338, <https://doi.org/10.1016%2Fj.energy.2015.11.034>
- [84] Alford T, Gadre MJ, Vemuri RN, Theodore ND (2012) Susceptor-assisted microwave annealing for activation of arsenic dopants in silicon. *Thin Solid Films* 520(13):4314–4320, <https://doi.org/10.1016%2Fj.tsf.2012.02.086>
- [85] Gutmann B, Obermayer D, Reichart B, Prekodravac B, Irfan M, Kremser JM, Kappe CO (2010) Sintered silicon carbide: a new ceramic vessel material for microwave chemistry in single-mode reactors. *Chem A Eur J* 16(40):12182–12194, <https://doi.org/10.1002%2Fchem.201001703>
- [86] Wuchina E, Opila E, Opeka M, Fahrenholtz W, Talmy I (2007) Uhtcs: ultra-high temperature ceramic materials for extreme environment applications. *Electrochem Soc Interface* 6(4):30. <https://link.springer.com/article/10.1007/s10853-018-3101-y#ref-CR45>
- [87] Schleppe, J., Gibbons, J., Groetsch, A. et al. Manufacture of glass and mirrors from lunar regolith simulant. *J Mater Sci* 54, 3726–3747 (2019). <https://doi.org/10.1007/s10853-018-3101-y>
- [88] Tréguer, Paul J.; De La Rocha, Christina L. (2013-01-03). The World Ocean Silica Cycle. *Annual Review of Marine Science*. 5 (1): 477–501. doi:10.1146/annurev-marine-121211-172346
- [89] Yool, A., and Tyrrell, T. (2003), Role of diatoms in regulating the ocean's silicon cycle, *Global Biogeochem. Cycles*, 17, 1103, <https://doi.org/10.1029/2002GB002018>
- [90] Conley, D. J., Terrestrial ecosystems and the global biogeochemical silica cycle, *Global Biogeochem. Cycles*, 16( 4), 1121, 2002, <https://doi.org/10.1029/2002GB001894>
- [91] Qin, X., Liu, J. H., Zhao, W. S., Chen, X. J., Guo, Z. J., Peng, Y. L. (2013). Gibberellin 20-oxidase gene OsGA20ox3 regulates plant stature and disease development in rice. *Mol. Plant Microbe In.* 26, 227–239. <https://doi.org/10.1094/MPMI-05-12-0138-R>
- [92] Meena, V.D., Dotaniya, M.L., Coumar, V. et al. A Case for Silicon Fertilization to Improve Crop Yields in Tropical Soils. *Proc. Natl. Acad. Sci., India, Sect. B Biol. Sci.* 84, 505–518 (2014). <https://doi.org/10.1007/s40011-013-0270-y>
- [93] Liang, Y., Chen, Q. I. N., Liu, Q., Zhang, W., Ding, R. (2003). Exogenous silicon (Si) increases antioxidant enzyme activity and reduces lipid peroxidation in roots of salt-stressed barley (*Hordeum vulgare* L.). *J. Plant Physiol.* 160, 1157–1164. <https://doi.org/10.1078/0176-1617-01065>
- [94] Fauteux, F., Rémus-Borel, W., Menzies, J. G., Bélanger, R. R. (2005). Silicon and plant disease resistance against pathogenic fungi. *FEMS Microbiol. Lett.* 249, 1–6. <https://doi.org/10.1016/j.femsle.2005.06.034>
- [95] Cai, K., Gao, D., Luo, S., Zeng, R., Yang, J., Zhu, X. (2008). Physiological and cytological mechanisms of silicon-induced resistance in rice against blast disease. *Physiol. Plantarum.* 134, 324–333. <https://doi.org/10.1111/j.1399-3054.2008.01140.x>
- [96] Yavaş, İ., Aydın, Ü.N.A.Y. (2017). The Role of Silicon under Biotic and Abiotic Stress Conditions. *Türkiye Tarımsal Araştırmalar Dergisi* 4, 204–209. <https://doi.org/10.19159/tutad.300023>
- [97] Aizenberg, Joanna et al. (2005). Skeleton of *Euplectella* sp: Structural Hierarchy from the Nanoscale to the Macroscale. *Science* (New York, N.Y.) 309, 275-8. <http://dx.doi.org/10.1126/science.1112255>
- [98] Kröger, Nils, and Nicole Poulsen. Diatoms-from cell wall biogenesis to nanotechnology. *Annual review of genetics* vol. 42 (2008): 83-107. <https://doi.org/10.1146/annurev.genet.41.110306.130109>
- [99] De Martino A., et al. Physiological and molecular evidence that environmental changes elicit morphological interconversion in the model diatom *Phaeodactylum tricoratum*. *Protist.* 2011;162:462–481. <https://doi.org/10.1016/j.protis.2011.02.002>
- [100] Pančić M., Torres R.R., Almeda R., Kiorboe T. Silicified cell walls as a defensive trait in diatoms. *Proc. R. Soc. B Biol. Sci.* 2019;286:20190184. <https://doi.org/10.1098/rspb.2019.0184>
- [101] Durkin, C. A., Koester, J. A., Bender, S. J., & Armbrust, E. V. (2016). The evolution of silicon transporters in diatoms. *Journal of phycology*, 52(5), 716–731. <https://doi.org/10.1111/jpy.12441>
- [102] Shrestha, R. P., & Hildebrand, M. (2015). Evidence for a regulatory role of diatom silicon transporters in cellular silicon responses. *Eukaryotic cell*, 14(1), 29–40. <https://doi.org/10.1128/EC.00209-14>

- [103] Parkinson, John and Richard Gordon. Beyond micromachining: the potential of diatoms. *Trends in biotechnology* 17 5 (1999): 190-6 <https://doi.org/10.1016/S0167-7799%2899%2901321-9>
- [104] Nassif, Nadine and Jacques Livage. From diatoms to silica-based biohybrids. *Chemical Society reviews* 40 2 (2011): 849-59 <https://doi.org/10.1039/c0cs00122h>
- [105] Sethi, D., Butler, T. O., Shuhaili, F., & Vaidyanathan, S. (2020). Diatoms for Carbon Sequestration and Bio-Based Manufacturing. *Biology*, 9(8), 217. <https://doi.org/10.3390/biology9080217>
- [106] Butler T., Kapoore R.V., Vaidyanathan S. *Phaeodactylum tricornutum*: A Diatom Cell Factory. *Trends Biotechnol.* 2020;38:606–622. doi: 10.1016/j.tibtech.2019.12.023
- [107] Smetacek, V., Klaas, C., Strass, V. et al. Deep carbon export from a Southern Ocean iron-fertilized diatom bloom. *Nature* 487, 313–319 (2012). <https://doi.org/10.1038/nature11229>
- [108] Bullis, K. (2020, April 2). Silicon and sun. MIT Technology Review. Retrieved January 1, 2022, from <https://www.technologyreview.com/2006/11/01/227587/silicon-and-sun/>
- [109] Otzen, Daniel, The role of proteins in biosilicification, *Scientifica* vol. 2012 (2012): 867562. <https://doi.org/10.6064/2012/867562>
- [110] Richard Gordon, Ryan W. Drum, *The Chemical Basis of Diatom Morphogenesis*, International Review of Cytology, Academic Press, Volume 150, 1994, Pages 243-372, ISSN 0074-7696, [https://doi.org/10.1016/S0074-7696\(08\)61544-2](https://doi.org/10.1016/S0074-7696(08)61544-2)
- [111] Meena, V. D., Dotaniya, M. L., Coumar, V. (2014a). A case for silicon fertilization to improve crop yields in tropical soils. *Proc. Natl. Acad. Sci. India.* 84, 505. <https://doi.org/10.1007/s40011-013-0270-y>
- [112] Wang, R. R., Wang, Q., He, L. Y., Qiu, G., Sheng, X. F. (2015). Isolation and the interaction between a mineral-weathering *Rhizobium tropici* Q34 and silicate minerals. *World J. Microbiol. Biotechnol.* 31, 747–753. <https://doi.org/10.1007/s11274-015-1827-0>
- [113] Kang, S. M., Waqas, M., Shahzad, R., You, Y. H., Asaf, S., Khan, M. A., et al. (2017). Isolation and characterization of a novel silicate-solubilizing bacterial strain *Burkholderia eburnea* CS4-2 that promotes growth of japonica rice (*Oryza sativa* L. cv. Dongjin). *J. Soil Sci. Plant Nutr.* 63, 233–241. <https://doi.org/10.1080/00380768.2017.1314829>
- [114] Kumawat, N., Kumar, R., Kumar, S., Meena, V. S. (2017). Nutrient solubilizing microbes (NSMs): its role in sustainable crop production. In book agriculturally important microbes for sustainable agriculture. Springer, 25–61. [https://doi.org/10.1007/978-981-10-5343-6\\_2](https://doi.org/10.1007/978-981-10-5343-6_2)
- [115] Chandrakala, C., Voleti, S. R., Bandeppa, S., Kumar, N. S., Latha, P. C. (2019). Silicate solubilization and plant growth promoting potential of *rhizobium* Sp. isolated from rice rhizosphere. *Silicon*, 11, 1–12. <https://doi.org/10.1007/s12633-019-0079-2>
- [116] Lee, K. E., Adhikari, A., Kang, S. M., You, Y. H., Joo, G. J., Kim, J. H., et al. (2019). Isolation and Characterization of the High Silicate and Phosphate Solubilizing Novel Strain *Enterobacter ludwigii* GAK2 that Promotes Growth in Rice Plants. *Agronomy* 9, 144. <https://doi.org/10.3390/agronomy9030144>
- [117] Bist V, Niranjana A, Ranjan M, Lehri A, Seem K, Srivastava S. Silicon-Solubilizing Media and Its Implication for Characterization of Bacteria to Mitigate Biotic Stress. *Front Plant Sci.* 2020;11:28. Published 2020 Feb 28. <https://dx.doi.org/10.3389%2Ffpls.2020.00028>
- [118] Shabbir, Imran & Abd Samad, Mohd & Othman, Radziah & Wong, Mui-Yun & Sulaiman, Zulkefly & Jaafar, Noraini & Bukhari, Syed. (2020). Silicate solubilizing bacteria UPMSSB7, a potential biocontrol agent against white root rot disease pathogen of rubber tree. *Journal of Rubber Research.* 23. 1-9. <http://dx.doi.org/10.1007/s42464-020-00052-w>
- [119] Yahaya, S. & Aisha, B.M & Zegeye, Asfaw & Manning, David & Claire, Fialips. (2019). Bioleaching of silica sand using bio-reducing bacteria (*Shewanella* strains). *Bayero Journal of Pure and Applied Sciences.* 11. 93. <http://dx.doi.org/10.4314/bajopas.v11i1.16S>
- [120] Zahra Etamadifar, Shekoofeh Sadat Etamadzadeh & Giti Emtiazi (2019) A Novel Approach for Bioleaching of Sulfur, Iron, and Silica Impurities from Coal by Growing and Resting Cells of *Rhodococcus* spp, *Geomicrobiology Journal*, 36:2, 123-129, <https://doi.org/10.1080/01490451.2018.1514441>
- [121] Doke, S.D., Patel, C.M. & Lad, V.N. Improving physical properties of silica aerogel using compatible additives. *Chem. Pap.* 75, 215–225 (2021). <https://doi.org/10.1007/s11696-020-01281-4>
- [122] Vivod, Stephanie et al. (2008). Carbon nanofiber incorporated silica based aerogels with di-isocyanate cross-linking. *American Chemical Society, Polymer Preprints, Division of Polymer Chemistry.* 49. 306-307.
- [123] Śłosarczyk, Agnieszka. Carbon Fiber-Silica Aerogel Composite with Enhanced Structural and Mechanical Properties Based on Water Glass and Ambient Pressure Drying. *Nanomaterials (Basel, Switzerland)* vol. 11,2 258. 20 Jan. 2021, <https://doi.org/10.3390/nano11020258>
- [124] [https://www.academia.edu/1258759/Improvements\\_to\\_the\\_Synthesis\\_of\\_Polyimide\\_Aerogels](https://www.academia.edu/1258759/Improvements_to_the_Synthesis_of_Polyimide_Aerogels)
- [125] S.C. Jana, M.A.B. Meador, J.P. Randall, Process for forming shape-memory polymer aerogel composites, US Patent 0144962, (2010).
- [126] Maleki, Hajar & Durães, Luisa & Portugal, Antonio. (2014). An Overview on Silica Aerogels Synthesis and Different Mechanical Reinforcing Strategies. *Journal of Non-Crystalline Solids.* 385. 55–74. <http://dx.doi.org/10.1016/j.jnoncrsol.2013.10.017>
- [127] Meador, Mary Ann B. et al. Highly Porous and Mechanically Strong Ceramic Oxide Aerogels. US Patent US7732496B1 (2010). <https://patents.google.com/patent/US7732496B1/en>
- [128] Afroze, Jannatul & Tong, Liyong & Abden, Md & Yuan, Ziwen & Chen, Yuan. (2021). Hierarchical honeycomb graphene aerogels reinforced by carbon nanotubes with multifunctional mechanical and electrical properties. *Carbon.* 175. <http://dx.doi.org/10.1016/j.carbon.2021.01.002>
- [129] Aron Newman and Fred Lauten, Sprayable Aerogel Insulation US patent US20080241490A1 (2008). <https://patents.google.com/patent/US20080241490A1/en>
- [130] Lin Liu, Zihé Cai, Shengxuan Lin, and Xiaobin Hu, Frozen Spray-Coating Prepared Graphene Aerogel with Enhanced Mechanical, Electrochemical, and Electromagnetic Performance for Energy Storage, *ACS Applied Nano Materials* 2018 1 (9), 4910-4917. <https://doi.org/10.1021/acsanm.8b01091>
- [131] Ou, Danny et al. Sprayable Aerogel Bead Compositions With High Shear Flow Resistance and High Thermal Insulation Value. (2013). <https://ntrs.nasa.gov/archive/nasa/casi.ntrs.nasa.gov/20130012683.pdf>
- [132] Adams, Jr., et al., Revolutionary Concepts of Radiation Shielding for Human Exploration of Space, NASA TM 213688, 2005. [https://www.lpi.usra.edu/lunar/strategies/AdamsEtAl\\_NASA%20TM-2005-213688.pdf](https://www.lpi.usra.edu/lunar/strategies/AdamsEtAl_NASA%20TM-2005-213688.pdf)